correction date 24-02-2014

Ab initio thermodynamic and thermophysical properties of sapphirine end-members in the join $Mg_4Al_8Si_2O_{20}$ – $Mg_3Al_{10}SiO_{20}$

Donato Belmonte [(1)] , Giulio Ottonello [(1)] and Marino Vetuschi Zuccolini [(1)]

[(1)] DISTAV, Università di Genova, Corso Europa 26, 16132 Genova, Italy.

E-mails: donato.belmonte@unige.it, giotto@dipteris.unige.it, zucco@dipteris.unige.it

ABSTRACT

Using the hybrid B3LYP density functional method, we computed the *ab initio* thermodynamic and thermophysical properties of two sapphirine end-members, $Mg_4Al_8Si_2O_{20}$ (sapphirine-442) and $Mg_3Al_{10}SiO_{20}$ (sapphirine-351), in the join $Mg_3(Mg_{1-X}Al_X)Al_8(Al_XSi_{1-X})SiO_{20}$ with X = 0 - 1. Static and vibrational calculations performed in the framework of the quasi-harmonic approximation allowed to define the equation of state (EOS), elastic constant tensor, seismic velocities, IR spectra, mode Grüneisen parameters and thermodynamic properties of both sapphirine end-members. A modified Kieffer's model was adopted to evaluate the optic and acoustic mode contributions to thermodynamic functions stemming from *ab initio* phonon frequencies and directionally averaged seismic velocities, respectively. The extrinsic stability and liquidus phase relations of sapphirine were investigated in the model system MgO-Al_2O_3-SiO_2 (MAS) at different pressure conditions by coupling first principles calculations with the Hybrid Polymeric Approach (HPA) for multicomponent liquids and minimizing the Gibbs free energy of liquid and solid phases through the convex-hull analysis of equipotential surfaces. According to our thermodynamic modeling, sapphirine turns out to have a small field of primary crystallization in the MAS ternary diagram at 1-bar pressure, which becomes larger due to pressure effects up to 10 kbar, then progressively shrinks and disappears above 21 kbar.

Keywords: Sapphirine, thermodynamic properties, ab initio calculations, elasticity, equation of state, liquidus phase relations.

INTRODUCTION

Sapphirine is widely recognized as a key mineralogical phase in ultra-high temperature metamorphism of amphibolite to granulite facies rocks (Christy 1989a, 1989b; Grew et al. 1994). Nevertheless, its stability extends over a wide range of P-T conditions (Schreyer, 1968; Schreyer and Seifert 1969a, 1969b; Seifert 1974; Ackermand et al. 1975) and diverse bulk rock compositions as well. Gasparik (1994, 2000) carried out a comprehensive analysis of experimental phase relations in simplified mantle compositions pointing out that the role of sapphirine in determining the subsolidus phase relations of MgO-Al_2O_3-SiO_2 (MAS) and CaO-MgO-Al_2O_3-SiO_2 (CMAS) systems cannot be overlooked, especially at high pressures and temperatures. Furthermore, several studies show that sapphirine has a small field of primary crystallization at 1-bar pressure in the MAS ternary system (Foster 1950; Keith and Schairer 1952; Osborn and Muan 1960; Smart and Glasser 1976; Brigida et al. 2007), making it a relevant phase for refractory ceramics. It is interesting to note that pressure effects possibly widen the primary stability field of sapphirine in MAS or more complex systems (Taylor 1973; Liu and Presnall 1990, 2000; Milholland and Presnall 1998; Liu and O'Neill 2004), so that this mineral may be plausibly involved in basalt petrogenesis.

A remarkable feature of sapphirine is the use as a possible geothermobarometer, with Si-rich and Al-poor compositions (approaching a stoichiometric ratio $MgO : Al_2O_3 : SiO_2 = 2 : 2 : 1$) stable at higher pressures and possibly lower temperatures than Si-depleted and Al-enriched compositions (approaching a stoichiometric ratio $MgO : Al_2O_3 : SiO_2 = 3.5 : 4.5 : 1.5$, up to $3 : 5 : 1$), as supported by experimental phase equilibria (Schreyer and Seifert 1969a; Taylor 1973; Seifert 1974; Bishop and Newton 1975), crystal chemical considerations (Higgins et al. 1979) and natural occurrences (Grew et al. 2008). However, a quantitative evaluation on the basis of reliable

thermodynamic data for sapphirine has never been attempted and the compositional effects on its relative phase stability still remain uncertain.

In spite of its geological and mineralogical significance, the thermodynamic and thermophysical properties of sapphirine are poorly defined and largely unknown. At present only few calorimetric investigations exist (Charlu et al. 1975; Kiseleva and Topor 1975; Kiseleva 1976) but the interpretation of experimental results is not straightforward owing to the incomplete understanding of mixing properties, cation and stacking disorder (i.e. polytypism) in natural and synthetic samples. Conversely, fundamental properties of sapphirine such as elasticity, thermal expansion and equation of state (EOS) parameters are still unknown. In the last two decades a number of thermodynamic assessments appeared in the literature trying to give a quantitative appraisal of the subsolidus and melting phase relations of sapphirine-bearing assemblages in multicomponent systems at both ambient and non-ambient P-T conditions (Gasparik 1994, 2000; Gottschalk 1997; Logvinkov et al. 2001; Kelsey et al. 2004; Jung et al. 2004; Mao et al. 2005; Podlesskii et al. 2008; Podlesskii 2010; Holland and Powell 2011). Although all these assessments are internally-consistent, the inferred thermodynamic properties are model-dependent and affected by evident drawbacks. Jung et al. (2004), for instance, define the properties of a sapphirine with 23 oxygens in the chemical formula (i.e. $Mg_4Al_{10}Si_2O_{23}$), which is quite incompatible with the exact 7:10 cation:oxygen ratio derived from structure determinations by X-ray and neutron diffraction (Moore 1969; Higgins and Ribbe 1979; Merlino 1980).

In this contribution, we present a density functional theory (DFT) based *ab initio* computational study on the thermodynamic, thermoelastic and equation of state parameters of sapphirine end-members in the join $Mg_4Al_8Si_2O_{20}$-$Mg_3Al_{10}SiO_{20}$. The aim of the calculated properties is to get new insights into the extrinsic stability and phase relations of sapphirine at high pressure and temperature conditions. The MAS ternary system was taken as reference phase diagram to define the topology of the primary stability field of sapphirine up to pressures of about

20 kbar and model its liquidus phase relations and high-pressure crystallization processes (see Implications Section).

COMPUTATIONAL METHOD

Calculations were performed with the periodic *ab initio* CRYSTAL09 code (Dovesi et al. 2009) adopting an all-electron Gaussian-type basis set and the hybrid B3LYP functional, which combines the Becke three-parameter hybrid exchange functional (Becke, 1993) with the Lee-Yang-Parr gradient-corrected correlation functional (Lee et al. 1988). Magnesium, silicon, aluminum and oxygen were described by 85-11G(d), 88-31G(d), 85-11G(d) and 8-411G(d) contractions, respectively (McCarthy and Harrison 1994; Catti et al. 1994; Nada et al. 1996). The exponents of the most diffuse *sp* and *d* shells were re-optimized as in our previous investigations to better account for the periodicity of the investigate systems (Ottonello et al. 2009a, 2009b, 2010a; Belmonte et al. 2013).

Cut-off limits in the evaluation of the Coulomb and Hartree-Fock exchange series are controlled by five parameters (see Dovesi et al. 2009) that were set to 8 8 8 8 18 to improve the numerical accuracy. The threshold on the self-consistent field (SCF) energy was set to 10^{-8} Hartree for the geometry optimization, and to 10^{-10} Hartree for the vibrational frequencies calculation. The reciprocal space was sampled according to a regular sublattice with shrinking factor IS = 3 (see Dovesi et al. 2009), corresponding to 10 **k** vectors in the irreducible part of the Brillouin zone (Monkhorst and Pack 1976). The DFT exchange-correlation contribution was evaluated by numerical integration over the unit cell volume. Radial and angular points of the atomic grid were generated through Gauss-Legendre and Lebedev quadrature schemes and grid pruning was applied, as discussed by Pascale et al. (2004). In this work, we used a pruned grid with 75 radial and 974 angular points. Details about the grid generation, the number of points in the reciprocal space and their influence on the accuracy and cost of calculation can be found in Gill et al. (1993) and Pascale et al. (2004).

Thermodynamic modeling of the MAS ternary system was performed at different pressure conditions by coupling *ab initio* calculations on sapphirine with the Hybrid Polymeric Approach (HPA) for multicomponent liquids (Ottonello 2001, 2005). The algorithm of the procedure along with the standard state properties of the chemical components at liquid state are described in full detail in Ottonello et al. (2013). Thermodynamic properties of the other solid phases nucleating in the MAS system were taken from the database of Berman (1988), while compressibility and thermal expansion data were taken from Saxena et al. (1993), except for mullite (Schneider and Eberhard 1990; Palko et al. 2002), cordierite (Tohill et al. 1999; Haussühl et al. 2011), periclase (Belmonte, 2013) and corundum (Belmonte et al. 2013). The Gibbs free energy values of the solid phases and the liquid have been calculated at each pressure conditions on a regular grid of temperature-composition (T-X) points in the range T = 1273 - 3273 K, then minimized through the convex-hull analysis of equipotential surfaces and interpolation of sample points by lifted Delaunay triangulation (Natali et al. 2010, 2013; see also Supplementary Materials in Ottonello et al. 2013). A step size of 5 K and a discretized grid of 4×10^6 points were used to sample the T-X space.

RESULTS AND DISCUSSION

Crystal structure: static calculations and equation of state

Sapphirine is a chain silicate with simplified general formula $M_8T_6O_{20}$, where M and T represent octahedral and tetrahedral sites, respectively (Deer et al., 1997). Two different structural modifications, related to the OD character of the mineral (Merlino 1973; Merlino and Pasero 1997), have been proposed in the literature: a monoclinic 2*M* polytype with eight independent octahedral sites (M1, M2, M3, M4, M5, M6, M7 and M8) and six independent tetrahedral sites (T1, T2, T3, T4, T5 and T6) (Moore 1969); a triclinic 1*A* polytype with a different stacking sequence and an additional independent octahedral site (M9) (Merlino 1980). A further structural complexity is represented by the degree of cation ordering on M and T sites, for which there is no a general

consensus among different structural determinations (Moore 1969; Higgins and Ribbe 1979; Merlino 1980; Christy et al. 1992). If only MgO-Al_2O_3-SiO_2 compositions are taken into account, Mg and Al atoms are distributed over octahedral sites, while Al and Si atoms occupy tetrahedral sites. Compositional variations may occur along the binary join according to the Tschermak-type coupled subsitution:

$$^{M}Mg^{2+} + {}^{T}Si^{4+} = {}^{M}Al^{3+} + {}^{T}Al^{3+} \qquad (1)$$

The 2*M* polytype of sapphirine has a monoclinic structure, space group $P2_1/a$, with 136 atoms in the primitive unit cell (Z=4 for the 20-oxygen formula unit), all in the general position. For this study, we consider two sapphirine end-member compositions, sapphirine-442 ($Mg_4Al_8Si_2O_{20}$) and sapphirine-351 ($Mg_3Al_{10}SiO_{20}$). Disorder in our model structures occurs on only one M site and one T site. Thus, the two end-members considered in this study correspond to X=0 and X=1 points on the hypothetical solid solution $[Mg_3Al_4(Mg_{1-X}Al_X)]^M[Al_4Si(Al_XSi_{1-X})]^TO_{20}$. Since the most part of sapphirine natural compositions fall on the join $Mg_4Al_8Si_2O_{20}$–$Mg_3Al_{10}SiO_{20}$ (Higgins et al. 1979; Deer et al. 1997; Grew et al. 2008), these end-member compositions are often assumed for thermodynamic modeling in the MAS system (Logvinkov et al. 2001; Kelsey et al. 2004; Mao et al. 2005; Podlesskii et al. 2008; Podlesskii 2010; Holland and Powell 2011). We have (Mg,Al) disorder exclusively on the M3 site and (Al,Si) on T3. This apparent oversimplification is supported by the evidence that natural samples seem to be highly ordered (Moore 1969; Merlino 1980) and the degree of cation disorder turns out to be poorly constrained by different experimental determinations. While, for instance, T2 sites are affected by a certain amount of disorder according to the structural refinements of Moore (1969) and Merlino (1980), the single-crystal neutron diffraction investigation of Higgins and Ribbe (1979) revealed an almost complete order on these sites, as well as on T4 sites (see Table 1). Nevertheless, there is general consensus that M3 and T3 are the most disordered sites, justifying our choice of structural models. The interpretation of the high-resolution ^{27}Al and ^{29}Si NMR spectra obtained by Christy et al. (1992) shows that there is a greater degree of short-range order of Al and Si than is apparent from the long-range average site

153 occupancies of the structure refinements. This is explained by mixing of local multisite
154 configurations rather than random mixing on individual sites. The total Si content on T2+T3 is
155 always > 1 in the structure refinements of Table 1, which implies that there must be a substantial
156 proportion of T2+T3 pairs that are (SiSi) as in our model for sapphirine-442, despite the
157 enthalpically unfavourable Si-O-Si link. Christy et al. (1992) note that more Si-rich compositions
158 are more disordered, which, along with the presence of significant Si on T4 and T6 in some of the
159 refinements of Table 1, suggest that other ordering variants of the 442 composition, e.g. with (SiSi)
160 on T2+T6 or on T3+T4, should be considered. To test this possibility, we performed static
161 calculations on a different 442 configuration, with Si atoms ordered on T2 and T6 instead of T2 and
162 T3 sites, assuming for simplicity that zero-point correction and thermal contributions were almost
163 unchanged. The total energy of the former configuration turns out to be ~0.1 kJ/mol lower than the
164 latter, in agreement with the increased proportion of Al-O-Si linkages in the structure with Si on
165 T2+T6. Nevertheless, the difference in total energy between these two configurations seems too
166 small to produce significant changes in the stability relations of sapphirine.

167 As far as the symmetry is concerned, our calculations focus on the monoclinic 2*M* polytype
168 only, since the investigation of the thermodynamic effects of stacking disorder, if any, is far beyond
169 the aim of this study. Note that the lower simmetry of the 1*A* polytype results in splitting of the M8
170 site into distinct M8 and M9 sites (Merlino 1980). Next-nearest neighbors are different for the two
171 MDO polytypes, which is also likely to cause differences in mixing behaviour. It certainly seems to
172 be the case that minor substituents like Fe^{2+}, Fe^{3+} and Be behave differently in the 1*A* and 2*M*
173 phases, evidenced by their stabilization effects (cf. Christy 1989a; Christy et al. 2002). In particular,
174 Christy (1989a) pointed out that 2*M* phase is stabilized by high temperature, and hence is likely to
175 be the stable alternative on the liquidus at the pressures considered in this study.

176 **Table 1**

177 Full geometry optimization, of both cell-edges and internal coordinates, was carried out with
178 a symmetry-preserving relaxation procedure implemented in the CRYSTAL09 code (Civalleri et al.

2001; Doll et al. 2004; Dovesi et al. 2009). The agreement between the calculated structural parameters and the experimental results obtained on natural samples (Moore 1969; Higgins and Ribbe 1979; Merlino 1980) is satisfactory (Table 1). The <M-O> and <T-O> mean bond distances listed in Table 2 show that the calculated values agree with those experimentally observed within 1% and 2% respectively, except for M3 and T3 sites which are assumed to be fully occupied either by Mg/Al or Si/Al atoms in our calculated structures. Nevertheless, the <M3-O> and <T3-O> mean bond distances refined by Moore (1969), Higgins and Ribbe (1979) and Merlino (1980) fall consistently within the *ab initio* values calculated for sapphirine-351 and sapphirine-442 in this work (Table 2). Furthermore, the <T2-O> and <T4-O> mean bond distances determined by Higgins and Ribbe (1979) (1.656 Å and 1.750 Å, respectively) are closer to the *ab initio* values (1.642÷1.643 Å and 1.771÷1.773 Å) than those refined by Moore (1969) (1.658 Å and 1.733 Å) and Merlino (1980) (1.66 Å and 1.73 Å). This is clearly consistent with the higher degree of Si/Al ordering on T2 and T4 sites observed by Higgins and Ribbe (1979) in their samples.

Table 2

The B3LYP volumes are slightly overestimated with respect to experiments due to the well-known effect of exchange-correlation functionals based on the generalized gradient approximation (GGA). The overestimation may be expected within 2-3% for alkali earth oxides and aluminosilicates (Corà et al. 2004; Demichelis et al. 2010; Ottonello et al. 2009a, 2010a). On the other hand, the inclusion of some fraction (20%) of non-local exact Hartree-Fock exchange in the hybrid density functional improves the quality of the calculated vibrational spectra, hence the thermodynamic accuracy for insulating crystalline solids, as pointed out by several recent computational works (Demichelis et al. 2010; De La Pierre et al. 2011; Többens and Kahlenberg 2011; Kaindl et al. 2012; Prencipe et al. 2012; Ulian et al. 2013).

Fitting the *ab initio* pressure-volume curves with a 3rd order finite strain Birch-Murnaghan equation of state (BM3-EOS) yields a static bulk modulus K_0 = 158.7 ± 0.6 GPa and a pressure derivative K'_0 = 4.68 ± 0.14 for sapphirine-442, K_0 = 172.3 ± 0.4 GPa and K'_0 = 4.28 ± 0.09 for

sapphirine-351 (Figure 1). As far as we know, these are the first determinations made so far and there are neither experimental nor other computational data to compare with. The ratios a/a_0, b/b_0 and c/c_0 predicted for sapphirine-442 and sapphirine-351 in the pressure range P = 0 ÷ 10 GPa are reported in Table 3. Both end-members display almost isotropic linear compressibilities, though minor differences along the *a*, *b*, *c* crystallographic axes may be inferred from the calculated values: *b* axis, for instance, turns out to be more compressible and less compressible than *a*, *c* axes in the sapphirine-442 and sapphirine-351 structures, respectively, up to pressures of 10 GPa (Table 3).

Table 3

Figure 1

Vibrational calculations

The calculation of the phonon frequencies at Γ point was performed within the harmonic approximation diagonalising the central zone (**k** = 0) mass-weighted Hessian matrix:

$$W_{ij}(\vec{k}=0) = \frac{H_{ij}}{\sqrt{M_i M_j}} \qquad (2)$$

where M_i and M_j are the atomic masses associated with the i,j-th cartesian coordinates and H_{ij} is the second derivative of the potential energy, evaluated at equilibrium (**u** = 0), with respect to the atomic displacements:

$$H_{ij} = \frac{1}{2}\left[\frac{\partial^2 V_{(x)}}{\partial u_i \partial u_j}\right]_0 \qquad (3)$$

In Equation 3, V(**x**) defines the potential energy surface (PES) of a periodic system with N nuclei (which is function of vector **x** of the 3N atomic coordinates), while $u_i = x_i - x_i^*$ and $u_j = x_j - x_j^*$ define the atomic displacements from the equilibrium positions (x_i^* and x_j^*). The optimized structure was taken as reference in the vibrational frequencies calculation. In the CRYSTAL code, first derivatives of the energy with respect to the atomic positions are calculated analytically for all

228 u_j coordinates (Doll 2001), while second derivatives at **u** = 0 (where all first derivatives are zero)
229 are calculated numerically. A more detailed description of the procedure can be found elsewhere
230 (cf. Pascale et al. 2004).

231 In both sapphirine-442 and sapphirine-351 monoclinic unit cells there are 136 atoms, hence
232 408 (= 3 × 136) vibrational modes (405 optic and 3 acoustic). The irreducible representations of the
233 optic modes at Γ point are:

234 $$\Gamma_{optic} = 101A_u + 102A_g + 102B_g + 100B_u \quad (4)$$

235 A total of 201 IR active modes (101 A_u + 100 B_u) and 204 Raman active modes (102 A_g + 102 B_g)
236 is then expected, along with three additional acoustic modes (1 A_u + 2 B_u) corresponding to rigid
237 translations of the lattice. The vibrational frequencies obtained in this study for both sapphirine end-
238 members, along with their relative mode Grüneisen parameters (see below) are listed in Tables A1
239 and A2 of Appendix I.

240 Integrated intensities for IR absorption (I_n) were computed for each n^{th} vibrational mode by
241 means of the mass-weighted effective Born charge vector evaluated through a Berry phase approach
242 (Dall'Olio et al. 1997). A graphical representation of the IR spectrum in the frequency range 0-1200
243 cm^{-1} was obtained as a superposition of Lorentzian functions, one for each mode, assuming a
244 damping factor of 30 cm^{-1} (see Figure 2, where the IR spectra experimentally measured on natural
245 samples by Christy et al. 1992 and Hofmeister and Bowey 2006 are also reported for comparison).
246 The choice of a constant damping factor was made to better appreciate the overall features of the
247 envelope and to aid a comparison between *ab initio* computations and experimental measurements,
248 the latter being unable to resolve the individual vibrational modes due to the large size and low
249 symmetry of the unit cell. As shown in Figure 2, the calculated IR spectrum of sapphirine-442
250 reproduce the position of the observed maxima in the experimental envelopes, which are clearly due
251 to a superposition of several IR-active modes. The weak peaks observed by Hofmeister and Bowey
252 (2006) in the low-frequency region and assigned to translations of Mg cations in the octahedral sites
253 of the structure are reproduced by our calculations. The mid- to high-frequency range of the

spectrum is dominated by internal bending and stretching modes, even though a one-by-one comparison with the experimental data is not feasible due to the large number and multiple overlapping of the bands. As pointed out by Hofmeister and Bowey (2006), the peak observed by Christy et al. (1992) between 1100 and 1200 cm^{-1} is probably a longitudinal optic (LO) mode since it does not correspond to any calculated frequency.

Figure 2

Acoustic and seismic properties

At the long-wavelength limit corresponding to the center of the Brillouin zone ($\mathbf{k}\rightarrow 0$) the first three solutions of the dispersion relation vanish (Born and Huang 1954). These solutions are related to the acoustic modes of the crystal and correspond to homogeneous translation of all the atoms in the structure along the three spatial directions by the effect of a polarized elastic wave. The phase velocity and polarization of the seismic wave along a given propagation direction are obtained by solving the well-known Christoffel determinant (Musgrave 1970):

$$\left| c_{ijkl} n_j n_l - \rho V^2 \delta_{ik} \right| = 0 \qquad (5)$$

where V is the phase velocity of the seismic wave, $\boldsymbol{n} = \boldsymbol{n}\ (n_x, n_y, n_z)$ the unit vector normal to the wave surface defining seismic propagation into space, c_{ijkl} the elastic constant tensor, ρ the density of the crystal and δ_{ik} a Kronecker delta. The solutions are of two types: a quasi-longitudinal wave with polarization nearly parallel to the direction of propagation (V_P), and two quasi-shear waves with polarization nearly perpendicular to n_i (V_{S1} and V_{S2}, the former propagating faster than the latter, i.e. $V_{S1} > V_{S2}$).

The components of the fourth-rank elastic constant tensor (c_{ijkl}) were computed using stress-strain relations as the 2nd derivatives of the energy with respect to the strain components, that is

278 $$c_{ij} = \frac{1}{V}\frac{\partial^2 E}{\partial\varepsilon_i \partial\varepsilon_j}\bigg|_0 \qquad (6)$$

279 In Equation 6 we adopt a Voigt notation for the indexes ($c_{11} \rightarrow c_1$, $c_{22} \rightarrow c_2$, $c_{33} \rightarrow c_3$, $c_{23} = c_{32} \rightarrow$
280 c_4, $c_{13} = c_{31} \rightarrow c_5$ and $c_{12} = c_{21} \rightarrow c_6$). Calculations were carried out by using an automatic scheme
281 implemented in the CRYSTAL09 code (Perger et al. 2009) and applying strains up to 0.02 in
282 magnitude. The thirteen independent elastic stiffnesses (c_{ij}) of sapphirine-442 and sapphirine-351
283 are listed in Table 4, along with the compliances (s_{ij}); details about the stiffnesses-compliances
284 conversion can be found in Nye (1957).

285 **Table 4**

286 Single-crystal azimuthal seismic anisotropy for longitudinal waves (A_P) and shear waves (A_S) may
287 then be obtained as (Karki et al. 2001; Mainprice 2007):

288 $$A_P = \left(\frac{V_{P,MAX} - V_{P,MIN}}{\overline{V}_P}\right)\times 100 \qquad (7.1)$$

289 $$A_S = \left(\frac{V_{S,MAX} - V_{S,MIN}}{\overline{V}_S}\right)\times 100 \qquad (7.2)$$

290 where V_{MAX} and V_{MIN} are the fastest and slowest longitudinal and shear velocities, respectively,
291 and $\overline{V}_P$ and $\overline{V}_S$ are isotropic seismic velocities averaged over all propagation directions (see
292 below). The obtained results are presented in Figure 3 by means of inverse pole figures plotted on
293 contoured stereograms using the CAREWARE package (Mainprice 1990) and show that sapphirine
294 has relatively high A_P (~15-16%) and very high A_S (~32-33%) maximum anisotropies with respect
295 to other common rock-forming silicates, like, among others, plagioclase (27% for A_P and A_S),
296 orthopyroxene (17% for A_P and 5% for A_S), hornblende (24% for A_P and 23% for A_S), cordierite
297 (7% for A_P and 14% for A_S), sillimanite (23% for A_P and 20% for A_S), andalusite (21% for A_P and
298 13% for A_S), diopside (24% for A_P and 14% for A_S), garnet (1% for A_P and A_S). Since sapphirine
299 it is likely a major consituent of mafic granulites in the lowermost continental crust (cf. Christy et

al. 1989b), it may contribute to the seismic velocity anisotropy of lower crust sections (Toohill et al. 1999 and references therein).

Figure 3

Directionally averaged shear and longitudinal velocities may be evaluated through the following scheme (Kieffer 1979a):

$$u_3 = V_{P,VRH} \qquad (8.1)$$

$$u_2 = \sqrt[3]{\frac{V_{S,VRH}^3 \cdot V_{S,MAX}^3}{2\left(V_{S,VRH}^3 + V_{S,MAX}^3\right)}} \qquad (8.2)$$

$$u_1 = \sqrt[3]{\frac{V_{S,VRH}^3 \cdot u_2^3}{\left(2u_2^3 - V_{S,VRH}^3\right)}} \qquad (8.3)$$

where $V_{S,MAX}$ is the fastest shear-wave velocity in the single-crystal, while $V_{P,VRH}$ and $V_{S,VRH}$ are the aggregate Voigt-Reuss-Hill longitudinal and shear seismic velocities (VRH; Hill 1952), obtained from the aggregate elastic moduli (bulk modulus and shear modulus) as follows:

$$K_V = \frac{1}{9} \times \left(c' + 2c''\right) \qquad (9.1)$$

$$K_R = \left(s' + 2s''\right)^{-1} \qquad (9.2)$$

$$\overline{K}_{VRH} = \frac{1}{2}\left(\mu_V + \mu_R\right) \qquad (9.3)$$

$$\mu_V = \frac{1}{15} \times \left(c' - c'' + 3c'''\right) \qquad (10.1)$$

$$\mu_R = 15 \times \left(4s' - 4s'' + 3s'''\right)^{-1} \qquad (10.2)$$

$$\overline{\mu}_{VRH} = \frac{1}{2}\left(\mu_V + \mu_R\right) \qquad (10.3)$$

$$\overline{V}_{S,VRH} = \sqrt{\overline{\mu}_{VRH} / \rho} \qquad (11)$$

$$\overline{V}_{P,VRH} = \sqrt{\frac{\overline{K}_{VRH} + \frac{4}{3} \times \overline{\mu}_{VRH}}{\rho}} \qquad (12)$$

K_V (and μ_V), K_R (and μ_R) in the above equations are the Voigt and Reuss bounds for bulk modulus (and shear modulus), respectively; ρ is the density; $c' = c_{11} + c_{22} + c_{33}$ and $c''' = c_{44} + c_{55} + c_{66}$ are obtained by summing up the diagonal terms of the stiffness tensor; $c'' = c_{12} + c_{13} + c_{23}$ is the sum of the non-diagonal terms of the stiffness tensor; $s' = s_{11} + s_{22} + s_{33}$ and $s''' = s_{44} + s_{55} + s_{66}$ are obtained by summing up the diagonal terms of the compliance tensor; $s'' = s_{12} + s_{13} + s_{23}$ is the sum of the non-diagonal terms of the compliance tensor.

As a proof of the internal consistency of the procedure one must verify that the static bulk modulus (K_0) obtained by fitting the P-V values with a BM3-EOS is not much dissimilar from the aggregate bulk modulus ($\overline{K}_{VRH}$) obtained through the Voigt-Reuss-Hill averaging procedure. We calculated $\overline{K}_{VRH}$ = 159.76 GPa (to be compared with K_0 = 158.73 GPa) for sapphirine-442 and $\overline{K}_{VRH}$ = 173.02 GPa (to be compared with K_0 = 172.33 GPa) for sapphirine-351.

Young's modulus (E) and Poisson's ratio (ν_P) are respectively:

$$E = \frac{9\overline{K}_{VRH}\overline{\mu}_{VRH}}{3\overline{K}_{VRH} + \overline{\mu}_{VRH}} \qquad (13)$$

$$\nu_P = \frac{3\overline{K}_{VRH} - 2\overline{\mu}_{VRH}}{2\times\left(3\overline{K}_{VRH} + \overline{\mu}_{VRH}\right)} \qquad (14)$$

The maximum frequency of each acoustic branch was obtained from the directionally averaged seismic velocities by applying:

$$\omega_i = \nu_i\left(\frac{6\pi N_0}{ZV}\right)^{1/3} \qquad (15)$$

where the term in brackets (k_{max}) defines the Brillouin zone boundary (i.e. the radius af a sphere with the same volume of the Brillouin zone, cf. Kieffer 1979c). Conversion of the obtained seismic velocities to linear frequencies yields the following results: ν_1 = 62.0 cm^{-1}, ν_2 = 68.9 cm^{-1}, ν_3 = 111.1 cm^{-1} for sapphirine-442; ν_1 = 63.5 cm^{-1}, ν_2 = 71.4 cm^{-1}, ν_3 = 114.9 cm^{-1} for sapphirine-351.

All the relevant thermophysical properties calculated for sapphirine-442 and sapphirine-351 (i.e. single-crystal, directionally averaged and aggregate elastic moduli and seismic velocities) are summarized in Table 5.

Table 5

Thermodynamic properties

Due to the large size and low symmetry of the unit cell of sapphirine, a modified Kieffer's model (Kieffer 1979a, 1979b, 1979c) was adopted to evaluate the optic and acoustic mode contributions to thermodynamic functions stemming from *ab initio* phonon frequencies and directionally averaged seismic velocities, respectively. Several studies proved that revisited versions of the Kieffer's model based on first principles and/or lattice dynamics calculations are a valid alternative to full phonon dispersion calculations for crystals with large unit cells, providing excellent results for different kind of minerals, such as silicates, carbonates, oxides and phosphates (Fleche 2002; Ottonello et al. 2009a, 2009b, 2010a, 2010b; Prencipe et al. 2011; Ungureanu et al. 2012; Jacobs et al. 2013; Belmonte et al. 2013).

Thermoelastic properties can be obtained from the quasi-harmonic expression of the αK_T product:

$$\alpha K_T = \frac{R}{ZV}\sum_{i=4}^{3n}\gamma_i e^{X_i}\left(\frac{X_i}{e^{X_i}-1}\right)^2 \qquad (16)$$

where R is the gas constant, V is the molar volume, Z is the number of formula units in the unit cell, n is the number of atoms in the unit cell and X_i is the undimensionalized frequency of the i^{th} vibrational mode ($X_i = h\omega_i/kT$, where h and k represent, respectively, Planck and Boltzmann constants and ω_i is the radial frequency). The mode Grüneisen parameters (γ_i) define the volume dependence of the 3n vibrational modes of the lattice in the framework of the quasi-harmonic approximation (QHA), being expressed as:

$$\gamma_i = -\frac{\partial \ln \nu_i}{\partial \ln V} \qquad (17)$$

where ν_i is the wavenumber of the vibrational frequencies (expressed in cm^{-1}). The numerical values of the mode Grüneisen parameters, obtained by fitting the results of phonon calculations at different compressed states with second-order polynomials, are listed in Tables A1 and A2 of Appendix I.

The product αK_T attains a fairly constant value at high temperature, averaging 0.0044 GPa/K for sapphirine-351 and 0.0042 GPa/K for sapphirine-442 in the range T = 1000 - 3000 K. Following the guidelines developed in our previous works (see for instance Ottonello et al. 2010a), we obtained $(\partial K_T/\partial T)_P$ = –210 bar/K for sapphirine-442 and $(\partial K_T/\partial T)_P$ = –188 bar/K for sapphirine-351. The calculated values for thermal expansivity are well reproduced by the following polynomial function:

$$\alpha_V(T) = \alpha_0 T + \alpha_1 + \alpha_2 T^{-1} + \alpha_3 T^{-2} + \alpha_4 T^{-3} \qquad (18)$$

The obtained coefficients are $\alpha_0 = 9.0302\times10^{-9}$; $\alpha_1 = 1.0411\times10^{-5}$; $\alpha_2 = 14.0340\times10^{-3}$; $\alpha_3 = -6.4469$; $\alpha_4 = 814.288$ (R^2=0.9999) for sapphirine-442 and $\alpha_0 = 6.0817\times10^{-9}$; $\alpha_1 = 1.5709\times10^{-5}$; $\alpha_2 = 8.2836\times10^{-3}$; $\alpha_3 = -4.3554$; $\alpha_4 = 547.232$ (R^2=1.0000) for sapphirine-351. As far as we know, there are no experimental data for thermal expansion of sapphirine. The thermal expansion coefficients calculated at ambient conditions (T=298.15 K, P = 1 bar) for sapphirine-442 ($\alpha_{298.15} = 1.84 \times 10^{-5}$ K^{-1}) and sapphirine-351 ($\alpha_{298.15} = 1.70 \times 10^{-5}$ K^{-1}, respectively) are rather different from the semi-empirical estimates taken from various thermodynamic assessments ($\alpha_{298.15} = 2.50 \times 10^{-5}$ K^{-1} according to Gottschalk 1997; $\alpha_{298.15} = 2.06 \times 10^{-5}$ K^{-1} according to Kelsey et al. 2004; $\alpha_{298.15} = 2.05 \times 10^{-5}$ K^{-1} according to Holland and Powell 2011).

In the harmonic approximation the isochoric heat capacity of one mole of a substance can be expressed as

$$C_V = \frac{3R}{Z}\left(\frac{2}{\pi}\right)^3 \sum_{i=1}^{3} \int_0^{X_i} \frac{[\arcsin(X/X_i)]^2 X^2 e^X dX}{\left(X_i^2 - X^2\right)^{1/2}\left(e^X - 1\right)^2} + \frac{R}{Z}\sum_{i=4}^{3n} e^{X_i}\left(\frac{X_i}{e^{X_i} - 1}\right)^2 \qquad (19)$$

The first term on the right of Equation 19 is the acoustic contribution at $\mathbf{k}_{max}$ represented in terms of a sine-wave dispersion relation (Kieffer 1979a, 1979b, 1979c), while the second term is the contribution of all the remaining (optic) modes. The computed isochoric heat capacity attains the Dulong-Petit limit (3nR) at high temperature, as expected from QHA.

Using the standard relation between C_p and C_v, i.e.:

$$C_P = C_V + TV_T\alpha_V^2 K_T \qquad (20)$$

we evaluated C_p and translated its T-dependency into the polynomial expression commonly adopted in metallurgy (cf. Ottonello et al. 2013):

$$C_P = a + b\times T + c\times T^{-2} + d\times T^{-1/2} + e\times T^{-3} + f\times T^{2} + g\times T^{3} \qquad (21)$$

Regression coefficients, valid between 298.15 and 3000 K, are as follows: a = 791.61; b = 0.065455; c = -18.175×10^{6}; d = -481.63; e = -0.91576×10^{9}; f = 0.34196×10^{-5}; g = -2.0517×10^{-9} for sapphirine-442; a = 789.73; b = 0.0603; c = -9.1751×10^{6}; d = -782.10; e = -3.1847×10^{9}; f = 1.327×10^{-5}; g = -5.1473×10^{-9} for sapphirine-351. The calculated heat capacities show a good agreement with the calorimetric results of Kiseleva and Topor (1975) and Kiseleva (1976), which are reproduced within 2% over the range T = 298.15 ÷ 1000 K (Figure 4). The inset of Figure 4 shows as the difference between the C_P values of the two sapphirine end-members are small (less than 14 J/mol×K in the temperature range from 298.15 K to 3000 K).

Figure 4

In the absence of configurational disorder, the entropy of one mole of a crystalline substance reduces to:

$$S = \frac{3R}{Z}\left(\frac{2}{\pi}\right)^3 \sum_{i=1}^{3}\int_0^{X_i} \frac{[\arcsin(X/X_i)]^2\, X dX}{\left(X_i^2 - X^2\right)^{1/2}\left(e^X - 1\right)} - \frac{3R}{Z}\left(\frac{2}{\pi}\right)^3 \sum_{i=1}^{3}\int_0^{X_i} \frac{[\arcsin(X/X_i)]^2}{\left(X_i^2 - X^2\right)^{1/2}} \ln\left(1 - e^{-X}\right) dX + \frac{R}{Z}\sum_{i=4}^{3n}\left(\frac{X_i}{e^{X_i} - 1} - \ln\left(1 - e^{-X_i}\right)\right) + \frac{R}{Z}\ln(Q_e) + \int_0^T V_T K_T \alpha_T^2 dT \qquad (22)$$

The first two terms on the right side of Equation 22 are the sine-wave dispersion contributions (acoustic modes) of the Kieffer's model, the third term is the contribution of the remaining 3n-3

411 (optic) modes, the fourth term is the electronic contribution arising from spin multiplicity (here
412 identically equal to zero) and the last term is the anharmonic contribution to the entropy of the
413 substance. It must be stressed that, since α_V was derived in the framework of QHA, the estimate of
414 the last integral in Equation 22 is a quasi-harmonic estimate as well. The standard state entropy
415 attains a value of S^0_{298} = 397.6 J/(mol×K) for sapphirine-351 and S^0_{298} = 407.0 J/(mol×K) for
416 sapphirine-442. Kiseleva (1976) gives a value of S^0_{298} = 412.0 J/(mol×K) for a synthetic sapphirine
417 with the same composition of sapphirine-442. It may be argued that the slightly higher value
418 reported by Kiseleva (1976) is likely due to a configurational contribution related to some
419 structural disorder in the synthetic sample (cf. Christy et al. 1992). This kind of contribution is
420 absent in our end-member compositions. If an ideal mixing of Mg and Al atoms in the M3
421 octahedral sites and Al and Si atoms in the T3 tetrahedral sites is considered, the configurational
422 contribution to entropy will be expressed by:

423 $$S_{mixing} = -R\sum_{i,j} N_i \left(X_{i,j} \ln X_{i,j}\right) \qquad (23)$$

424 where N_i is the number of sites of type *i* per formula unit and $X_{i,j}$ is the molar fraction of site *i*
425 occupied by the atomic species *j* (in our case *i* = M3, T3; *j* = Mg, Al, Si). According to Equation
426 23, the configurational entropy attains a maximum value of 11.53 J/(mol×K) in the case of a totally
427 random distribution of cations on M3 and T3 sites, a value which is consistent with the difference
428 between our calculated and the experimental S^0_{298} of sapphirine-442.

429 In the harmonic approximation the internal energy of a solid is given by:

430 $$U = E_{B3LYP,crystal} + \frac{3RT}{Z}\left(\frac{2}{\pi}\right)^3 \sum_{i=1}^{3} \int_0^{X_i} \frac{[\arcsin(X/X_i)]^2 X dX}{(X_i^2 - X^2)^{1/2}(e^X - 1)} + \frac{RT}{Z}\sum_{i=4}^{3n} X_i \left(\frac{1}{2} + \frac{1}{e^{X_i} - 1}\right) \qquad (24)$$

431 where the second and third terms on the right-hand side of Equation 24 represent the thermal
432 correction to U (ΔU_{T-0}, including the zero-point energy). Knowing U and S, the absolute enthalpy of
433 a substance (H) and the absolute values of its Helmholtz and Gibbs free energies (F and G,
434 respectively) may be obtained by the usual thermodynamic relations (H=U+PV; F=U-TS; G=H-

435 TS). These absolute values should not be confused with the enthalpy and free energy of formation
436 of a substance from the elements or oxides, that are the magnitudes usually provided by
437 thermodynamic tabulations. The calculation of the *ab initio* enthalpy of formation of a substance
438 from the elements at standard state requires the assessment of a thermochemical cycle of the type:

439 $$\overline{H}^{0}_{f,298.15} = \left(\Delta U_{298.15-0} + P\Delta V_{298.15-0}\right) - D_0 + \sum_{i=1}^{n/Z} n_i H_{f,A_i,0} - \sum_{i=1}^{n/Z} n_i \Delta H_{element_i,0\rightarrow 298.15} \qquad (25)$$

440 where the term in brackets is the thermal correction to the enthalpy at T = 298.15 K, $H_{f,A_i,0}$ is the
441 enthalpy of formation of the i^{th} gaseous atom from the stable element at T = 0 K, P = 1 bar (with the
442 summation extended to the n/Z atoms in the molecule; see Table 6), $\Delta H_{element_i,0\rightarrow 298.15}$ is the
443 enthalpy difference between T = 298.15 K and T = 0 K for the monatomic elements (Table 7) and
444 D_0 is the zero point dissociation energy of the gaseous molecule into gaseous atoms at 0 K:

445 $$D_0 = \sum_{i=1}^{n/Z} n_i E_{A_i} - \left(E_{B3LYP,crystal} + E_{ZPE,crystal}\right) \qquad (26)$$

446 corresponding to the difference between the sum of the electronic energies of the gaseous
447 atoms at 0 K and the electronic + zero point energy of the crystal (Table 7). The level of accuracy of
448 the thermochemical procedure has been discussed in details in previous works (see for instance
449 Ottonello et al. 2010a). As a rule of thumb, the procedure allows to reproduce enthalpies of
450 formation within 1-2% of uncertainty with respect to experimental data, essentially due to the
451 difficulty in estimating appropriate electronic energies for the isolated gaseous atoms (E_{Ai} terms in
452 Equation 26). In the case of sapphirine, E_{Ai} values have been optimized in order to reproduce the
453 correct heat content of the constituent oxides at standard state, taking as reference the $H^0_{f,298.15}$ of
454 periclase, corundum and quartz as defined by Robie and Hemingway (1995), Ditmars et al. (1982)
455 and Richet et al. (1982), respectively. Even though a direct comparison with observations is not
456 straightforward due to the non-negligible effect of structural disorder, the calculated values are in
457 reasonable agreement with those obtained by high-temperature solution calorimetry and the more
458 endothermic character of sapphirine-442 with respect to sapphirine-351 is consistent with the

459 calorimetric results produced so far on natural and synthetic samples (Charlu et al. 1975; Kiseleva
460 1976; Christy et al. 1992) (see Table 7). Enthalpies of formation of sapphirine-351 and sapphirine-
461 442 were raised within the limits of the theory in the thermodynamic modeling of MAS ternary
462 system (by 0.6% and 1.6%, respectively; see Table 7) in order to reproduce the ternary peritectic
463 points which define the primary field of crystallization of this mineral at 1-bar pressure. This is a
464 common practice in thermodynamic optimizations (e.g. Jung et al. 2004), especially when first
465 principle calculations are coupled with internally-consistent thermodynamic data assessed on
466 experimental phase equilibria (like those of Berman 1988). Since the MAS phase topology turns out
467 to be rather insensitive to the standard state molar volumes adopted for sapphirine, the *ab initio*
468 values were retained, although slightly overestimated (see Table 1).

469 **Table 6**

470 **Table 7**

471 The thermodynamic properties and thermophysical parameters of the two sapphirine end-
472 members investigated in this study are summarized in Table 8 and compared with literature data in
473 Table 9.

474 **Table 8**

475 **Table 9**

476

477 **IMPLICATIONS**

478 **Sapphirine as a "*liquidus*" phase in petrogenetic systems**

479 Ternary liquidus projections of the MAS system calculated for four different pressures are
480 given in Figure 5. For simplicity, the sapphirine solid solution is approximated by a mechanical
481 mixture of fixed-composition 351 and 442 end-members. Since a true solid solution will have a
482 lower free energy than the mechanical mixture of end-members, the stability field for sapphirine
483 calculated here represents necessarily a lower stability limit. At P = 1 bar, the thermodynamic
484 properties calculated in this work for sapphirine-351 are consistent with a small field of primary

485 crystallization matching experimental observations (Foster 1950; Keith and Schairer 1952; Osborn
486 and Muan 1960; Smart and Glasser 1976) (see Figure 5a). Raising the pressure to 5 kbar, both the
487 442 and 351 end-members becomes stable and the primary field of crystallization of sapphirine
488 considerably widens at the expenses of that of cordierite (Figure 5b). At P = 10 kbar, the field of
489 cordierite disappears and sapphirine persists as stable phase in the system (Figure 5c). Between 10
490 and 20 kbars, the field of sapphirine progressively shrinks up to disappear above P = 21 kbar. At
491 this pressure a primary phase field of pyrope garnet appears in the MAS system (Figure 5d). The
492 liquidus phase relations inferred by our thermodynamic modeling shed new light onto the P-T-X
493 effects on sapphirine stability giving a rationale to the few existing experimental results. First of all,
494 the experimental evidence that increasing pressure seems to stabilize less aluminous compositions
495 so that the Tschermak-type subsitution of (MgSi) for (AlAl) would be favoured by high pressure
496 conditions (Schreyer and Seifert 1969a; Taylor 1973; Seifert 1974; Bishop and Newton 1975;
497 Higgins et al. 1979) is here confirmed by the relative stability of sapphirine-351 and sapphirine-442
498 end-members in MAS system between 1 bar and 21 kbars. Secondly, the possibility to form
499 sapphirine by decomposition of cordierite (Schreyer and Seifert 1969b; Newton 1972) and/or
500 pyrope (Boyd and England 1959; Schreyer 1968; Schreyer and Seifert 1969a; Ackermand et al.
501 1975) is perfectly compatible with our modelled liquidus phase relations. Finally, the survival of a
502 noticeably large primary field of crystallization of sapphirine in MAS system up to relatively high-
503 pressure conditions (i.e. at least to P = 20 kbar) strengthens the hypothesis that sapphirine can be a
504 primary liquidus phase in basaltic magmas at high pressure, as already supported by some
505 experimental works (Taylor 1973; Liu and Presnall 1990, 2000; Milholland and Presnall 1998). The
506 recent discovery of igneous sapphirine as a product of melt-peridotite interaction at high pressure (~
507 1.1 GPa) in the Finero Phlogopite-Peridotite Massif of the Western Italian Alps (Giovanardi et al.
508 2013) is a natural evidence supporting this possibility.
509
510

ACKNOWLEDGMENTS

The constructive remarks of two anonymous reviewers improved the quality of the manuscript. This work has been partly supported by the MIUR-PRIN Project No. 2009B3SAFK (Topology of Phase Diagrams and Lines of Descent).

REFERENCES CITED

Ackermand, D., Seifert, F., and Schreyer, W. (1975) Instability of sapphirine at high pressures. Contributions to Mineralogy and Petrology, 50, 79-92.

Becke, A.D. (1993) Density-functional thermochemistry. III. The role of exact exchange. Journal of Chemical Physics, 98, 5648-5652.

Belmonte, D. (2013) Ab initio thermodynamics of deep mantle minerals: the system MgO-SiO_2, 253 p. Ph.D. thesis, University of Genova, Genova.

Belmonte, D., Ottonello, G., and Vetuschi Zuccolini, M. (2013) Melting of α-Al_2O_3 and vitrification of the undercooled alumina liquid: Ab initio vibrational calculations and their thermodynamic implications. Journal of Chemical Physics, 138, 064507. doi: 10.1063/1.4790612.

Berman, R.G. (1988) Internally-consistent thermodynamic data for minerals in the system Na_2O-K_2O-CaO-MgO-FeO-Fe_2O_3-Al_2O_3-SiO_2-TiO_2-H_2O-CO_2 . Journal of Petrology, 29, 445-522.

Bishop, F.C., and Newton, R.C. (1975) The composition of low-pressure synthetic sapphirine. Journal of Geology, 83, 511-517.

Born, M., and Huang, K. (1954) Dynamical theory of crystal lattices. Oxford University Press, Oxford.

Boyd, F.R., and England, J.L. (1959) Pyrope. Carnegie Institute of Washington Year Book, 58, 83-87.

Brigida, C., Poli, S., and Valle, M. (2007) High-temperature phase relations and topological constraints in the quaternary system MgO-Al_2O_3-SiO_2-Cr_2O_3: an experimental study. American Mineralogist, 92, 735-747.

538 Catti, M., Valerio, G., Dovesi, R., and Causà, M. (1994) Quantum-mechanical calculation of the
539 solid-state equilibrium $MgO+\alpha\text{-}Al_2O_3=MgAl_2O_4$ (spinel) versus pressure. Physical Review
540 B, 49, 14179-14187.

541 Charlu, T.V., Newton, R.C., and Kleppa, O.J. (1975) Enthalpies of formation at 970 K of
542 compounds in the system $MgO\text{-}Al_2O_3\text{-}SiO_2$ from high temperature solution calorimetry.
543 Geochimica et Cosmochimica Acta, 39, 1487-1497.

544 Chase, M.W.Jr. (1998) NIST – JANAF thermochemical tables, Journal of Physical and Chemical
545 Reference Data,, Monograph N. 9, American Chemical Society.

546 Christy, A.G. (1989a) The effect of composition, temperature and pressure on the stability of the
547 1*Tc* and 2*M* polytypes of sapphirine. Contributions to Mineralogy and Petrology, 103, 203-
548 215.

549 Christy, A.G. (1989b) The stability of sapphirine + clinopyroxene: implications for phase relations
550 in the $CaO\text{-}MgO\text{-}Al_2O_3\text{-}SiO_2$ system under deep-crustal and upper mantle conditions.
551 Contributions to Mineralogy and Petrology, 102, 422-428.

552 Christy, A.G., Phillips, B.L., Güttler, B.K., and Kirkpatrick, R.J. (1992) A ^{27}Al and ^{29}Si MAS NMR
553 and infrared spectroscopic study of Al-Si ordering in natural and synthetic sapphirine.
554 American Mineralogist, 77, 8-18.

555 Christy, A.G., Tabira, Y., Hölscher, A., Grew, E.S., Schreyer, W. (2002) Synthesis of beryllian
556 sapphirine in the system $MgO\text{-}BeO\text{-}Al_2O_3\text{-}SiO_2\text{-}H_2O$, and comparison with naturally
557 occurring beryllian sapphirine and khmaralite. Part 1: experiments, TEM and XRD.
558 American Mineralogist, 87, 1104-1112.

559 Civalleri, B., D'Arco, P., Orlando, R., Saunders, V.R., and Dovesi, R. (2001) Hartree-Fock
560 geometry optimisation of periodic systems with the CRYSTAL code. Chemical Physics
561 Letters, 348, 131-138.

562 Corà, F., Alfredsson, M., Mallia, G., Middlemiss, D.S., Mackrodt, W.C., Dovesi, R., and Orlando,
563 R. (2004) The performance of hybrid density functionals in solid state chemistry. In N.
564 Kaltsoyannis and J.E. McGrady, Eds., Principles and Applications of Density Functional
565 Theory in Inorganic Chemistry II, 113, p.171-232. Structure and Bonding, Springer-Verlag,
566 Berlin-Heidelberg.

567 Dall'Olio, S., Dovesi, R., and Resta, R. (1997) Spontaneous polarization as a Berry phase of the
568 Hartree-Fock wave function: The case of $KnbO_3$. Physical Review B, 56, 10105-10114.

569 Deer, W.A., Howie, R.A., and Zussman, J. (1997) Rock-forming Minerals, Single-Chain Silicates,
570 Volume 2A, 2nd ed., 668 p. The Geological Society, London.

571 De La Pierre, M., Orlando, R., Maschio, L., Doll, K., Ugliengo, P., and Dovesi, R. (2011)
572 Performance of six functionals (LDA, PBE, PBESOL, B3LYP, PBE0, and WC1LYP) in the
573 simulation of vibrational and dielectric properties of crystalline compounds. The case of
574 forsterite Mg_2SiO_4. Journal of Computational Chemistry, 32, 1775-1784.

575 Demichelis, R., Civalleri, B., Ferrabone, M., and Dovesi, R. (2010) On the performance of eleven
576 DFT functionals in the description of the vibrational properties of aluminosilicates.
577 International Journal of Quantum Chemistry, 110, 406-415.

578 Ditmars, D.A., Ihsihara, S., Chang, S.S., and Bernstein, G. (1982) Enthalpy and heat-capacity
579 standard reference material: synthetic sapphire (α-Al_2O_3) from 10 to 2250 K. Journal of
580 Research of the National Bureau of Standards, 87, 159-163.

581 Doll, K. (2001) Implementation of analytical Hartree-Fock gradients for periodic systems.
582 Computer Physics Communications, 137, 74-88.

583 Doll, K., Dovesi, R., and Orlando, R. (2004) Analytical Hartree-Fock gradients with respect to the
584 cell parameter for systems periodic in three dimensions. Theoretical Chemistry Accounts,
585 112, 394-402.

586 Dovesi, R., Saunders, V.R., Roetti, C., Orlando, R., Zicovich-Wilson, C.M., Pascale, F., Civalleri,
587 B., Doll, K., Harrison, N.M., Bush, I.J., D'Arco, P., and Llunell, M. (2009) CRYSTAL09
588 User's Manual, University of Torino, Torino.

589 Fleche, J.L. (2002) Thermodynamical functions for crystals with large unit cells such as zircon,
590 coffinite, fluorapatite, and iodoapatite from ab initio calculations. Physical Review B, 65,
591 245116.

592 Foster, W.R. (1950) Synthetic sapphirine and its stability relations in the system MgO-Al_2O_3-SiO_2.
593 Journal of Geology, 58, 135-151.

594 Gasparik, T. (1994) A petrogenetic grid for the system MgO-Al_2O_3-SiO_2. Journal of Geology, 102,
595 97-109.

596 Gasparik, T. (2000) An internally consistent thermodynamic model for the system CaO-MgO-
597 Al_2O_3-SiO_2 derived primarily from phase equilibrium data. Journal of Geology, 108, 103-
598 119.

599 Gill, P.M.W., Johnson, B.G., and Pople, J.A. (1993) A standard grid for density function
600 calculations. Chemical Physics Letters, 209, 506-512.

601 Giovanardi, T., Morishita, T., Zanetti, A., Mazzucchelli, M., and Vannucci, R. (2013) Igneous
602 sapphirine as a product of melt-peridotite interactions in the Finero Phlogopite-Peridotite
603 Massif, Western Italian Alps. European Journal of Mineralogy, 25, 17-31.

604 Gottschalk, M. (1997) Internally consistent thermodynamic data for rock-forming minerals in the
605 system SiO_2-TiO_2-Al_2O_3-Fe_2O_3-CaO-MgO-FeO-K_2O-Na_2O-H_2O-CO_2. European Journal of
606 Mineralogy, 9, 175-223.

607 Grew, E.S., Pertsev, N.N., Yates, M.G., Christy, A.G., Marquez, N., and Chernosky, J.V. (1994)
608 Sapphirine + forsterite and sapphirine + humite-group minerals in an ultra-magnesian lens

609 from Kuhi-lal, SW Pamirs, Tajikistan: are these assemblages forbidden? Journal of
610 Petrology, 35, 1275-1293.

611 Grew, E.S., Hålenius, U., Pasero, M., and Barbier, J. (2008) Recommended nomenclature for the
612 sapphirine and surinamite groups (sapphirine supergroup). Mineralogical Magazine, 72,
613 839-876.

614 Haussühl, E., Vinograd, V.L., Krenzel, T.F., Schreuer, J., Wilson, D.J., and Ottinger, J. (2011) High
615 temperature elastic properties of Mg-cordierite: experimental studies and atomistic
616 simulations. Zeitschrift für Kristallographie, 226, 236-253.

617 Higgins, J.B., and Ribbe, P.H. (1979) Sapphirine II: A neutron and X-ray diffraction study of (Mg-
618 Al)^{VI} and (Si-Al)^{IV} ordering in monoclinic sapphirine. Contributions to Mineralogy and
619 Petrology, 68, 357-368.

620 Higgins, J.B., Ribbe, P.H., and Herd, R.K. (1979) Sapphirine I: Crystal chemical contributions.
621 Contributions to Mineralogy and Petrology, 68, 349-356.

622 Hill, R.W. (1952) The elastic behaviour of a crystalline aggregate. Proceedings of the Physical
623 Society of London, 65 A, 349-354.

624 Hofmeister, A.M., and Bowey, J.E. (2006) Quantitative infrared spectra of hydrosilicates and
625 related minerals. Monthly Notices of the Royal Astronomical Society, 367, 577-591.

626 Holland, T.J.B., and Powell, R. (2011) An improved and extended internally consistent
627 thermodynamic dataset for phases of petrological interest, involving a new equation of
628 state for solids. Journal of Metamorphic Geology, 29, 333-383.

629 Jacobs, M.H.G., Schmid-Fetzer, R., and van den Berg, A.P. (2013) An alternative use of Kieffer's
630 lattice dynamics model using vibrational density of states for constructing thermodynamic
631 databases. Physics and Chemistry of Minerals, 40, 207-227.

632 Jung, I.-H., Decterov, S.A., and Pelton, A.D. (2004) Critical thermodynamic evaluation and
633 optimization of the MgO-Al_2O_3, CaO-MgO-Al_2O_3, and MgO-Al_2O_3-SiO_2 systems. Journal
634 of Phase Equilibria and Diffusion, 25, 329-345.
635 Kaindl, R., Többens, D.M., Penner, S., Bielz, T., Soisuwan, S., and Klötzer, B. (2012) Quantum
636 mechanical calculations of the vibrational spectra of quartz- and rutile-type GeO_2. Physics
637 and Chemistry of Minerals, 39, 47-55.
638 Karki, B.B., Stixrude, L., and Wentzcovitch, R.M. (2001) High-pressure elastic properties of major
639 materials of Earth's mantle from first principles. Reviews of Geophysics, 39, 507-534.
640 Keith, M.L., and Schairer, J.F. (1952) The stability field of sapphirine in the system MgO-Al_2O_3-
641 SiO_2. Journal of Geology, 60, 181-186.
642 Kelsey, D.E., White, R.W., Holland, T.J.B., and Powell, R. (2004) Calculated phase equilibria in
643 K_2O-FeO-MgO-Al_2O_3-SiO_2-H_2O for sapphirine-quartz-bearing mineral assemblages.
644 Journal of Metamorphic Geology, 22, 559-578.
645 Kieffer, S.W. (1979a) Thermodynamics and lattice vibrations of minerals: 1. Mineral heat
646 capacities and their relationships to simple lattice vibrational models. Reviews of
647 Geophysics and Space Physics, 17, 1-19.
648 Kieffer, S.W. (1979b) Thermodynamics and lattice vibrations of minerals: 2. Vibrational
649 characteristic of silicates. Reviews of Geophysics and Space Physics**,** 17, 20-34.
650 Kieffer, S.W. (1979c) Thermodynamics and lattice vibrations of minerals: 3. Lattice dynamics and
651 an approximation for minerals with application to simple substances and framework
652 silicates. Reviews of Geophysics and Space Physics, 17, 35-59.
653 Kiseleva, I.A. (1976) Thermodynamic parameters of the natural ordered and the synthetic
654 disordered sapphirines. Geokhimiya, 2, 189-201 (in Russian).
655 Kiseleva, I.A., and Topor, N.D. (1975) High-temperature heat capacity of sapphirine. Geokhimiya,
656 2, 312-315 (in Russian).

Lee, C., Yang, E., and Parr, R.G. (1988) Development of the Colle-Salvetti correlation-energy formula into a functional of the electron density. Physical Review B, 37, 785-789.

Liu, T.-C., and Presnall, D.C. (1990) Liquidus phase relationships on the join anorthite-forsterite-quartz at 20 kbar with applications to basalt petrogenesis and igneous sapphirine. Contributions to Mineralogy and Petrology, 104, 735-742.

Liu, T.-C., and Presnall, D.C. (2000) Liquidus phase relations in the system CaO-MgO-Al_2O_3-SiO_2 at 2.0 GPa: applications to basalt fractionation, eclogites, and igneous sapphirine. Journal of Petrology, 41, 3-20.

Liu, T.-C., and O'Neill, H.St.C. (2004) Partial melting of spinel lherzolite in the system CaO-MgO-Al_2O_3-SiO_2 ± K_2O at 1.1 GPa. Journal of Petrology, 45, 1339-1368.

Logvinkov, S.M., Semchenko, G.D., Kobyzeva, D.A., and Babushkin, V.I. (2001) Thermodynamics of phase relations in the subsolidus of the MgO-Al_2O_3-SiO_2 system. Refractories and Industrial Ceramics, 42, 434-439.

Mainprice, D. (1990) A FORTRAN program to calculate seismic anisotropy from the lattice preferred orientation of minerals. Computers and Geosciences, 16, 385-393.

Mainprice, D. (2007) Seismic anisotropy of the deep Earth from a mineral and rock physics perspective. In G.D. Price, Ed., Treatise on Geophysics, 2, p. 437-491. Elsevier, Amsterdam.

Mao, H., Fabrichnaya, O., Selleby, M., and Sundman, B. (2005) Thermodynamic assessment of the MgO-Al_2O_3-SiO_2 system. Journal of Materials Research, 20, 975-986.

McCarty, M.I., and Harrison, N.M. (1994) Ab initio determination of the bulk properties of MgO. Physical Review B, 49, 8574-8582.

Merlino, S. (1973) Polymorphism in sapphirine. Contributions to Mineralogy and Petrology, 41, 23-29.

Merlino, S. (1980) Crystal structure of sapphirine-1Tc. Zeitschrift für Kristallographie , 151, 91-100.

682 Merlino, S., and Pasero, M. (1997) Polysomatic approach in the crystal chemical study of minerals.
683 In S. Merlino, Ed., Modular Aspect of Minerals, 1, p. 297-312. EMU Notes in
684 Mineralogy, Eötvös University Press, Budapest.

685 Milholland, C.S., and Presnall, D.C. (1998) Liquidus phase relations in the CaO-MgO-Al_2O_3-SiO_2
686 system at 3.0 GPa: the aluminous pyroxene thermal divide and high-pressure fractionation
687 of picritic and komatiitic magmas. Journal of Petrology, 39, 3-27.

688 Monkhorst, H.J., and Pack, J.D. (1976) Special points for Brillouin-zone integrations. Physical
689 Review B, 13, 5188-5192.

690 Moore, P.B. (1969) The crystal structure of sapphirine. American Mineralogist, 54, 31-49.

691 Musgrave, M.J.P. (1970) Crystal Acoustics. Holden-Day, Boca Raton, Florida.

692 Nada, R., Nicholas, J. B., McCarthy, M.I., and Hess, A.C. (1996) Basis sets for ab initio periodic
693 Hartree-Fock studies of zeolite/adsorbate interactions: He, Ne, and Ar in silica sodalite.
694 International Journal of Quantum Chemistry, 60, 809-820.

695 Natali, M., Attene, M., and Ottonello, G. (2010) Modeling liquidus hypersurfaces through
696 simplicial complexes. In E. Puppo, A. Brogni and L. De Floriani, Eds., Proceedings of the
697 Eurographic Italian Chapter Conference, p. 1-6. The Eurographics Association, Goslar.

698 Natali, M., Attene, M., and Ottonello, G. (2013) Steepest descent paths on simplicial meshes of
699 arbitrary dimensions. Computers and Graphics, 37, 687-696.

700 Newton, R.C. (1972) An experimental determination of the high-pressure stability limits of
701 magnesian cordierite under wet and dry conditions. Jouranl of Geology, 80, 398-420.

702 Nye, J.F. (1957) Physical Properties of Crystals. Oxford University Press, Oxford.

703 Osborn, E.F., and Muan, A. (1960) Phase equilibrium diagrams of oxide systems. Plate 3. American
704 Ceramic Society with the Edward Orton Jr. Ceramic Foundation, Columbus, Ohio.

Ottonello, G. (2001) Thermodynamic constraints arising from the polymeric approach to silicate slags: the system CaO-FeO-SiO_2 as an example. Journal of Non-Crystalline Solids, 282, 72-85.

Ottonello, G. (2005) Chemical interactions and configurational disorder in silicate melts. Annals of Geophysics, 48, 561-581.

Ottonello, G., Civalleri, B., Ganguly, J., Vetuschi Zuccolini, M., and Noël, Y. (2009a) Thermophysical properties of the α-β-γ polymorphs of Mg_2SiO_4: a computational study. Physics and Chemistry of Minerals, 36, 87-106.

Ottonello, G., Vetuschi Zuccolini, M., and Civalleri, B. (2009b) Thermo-chemical and thermo-physical properties of stishovite: An ab-initio all-electron investigation. CALPHAD: Computer Coupling of Phase Diagrams and Thermochemistry, 33, 457-468.

Ottonello, G., Civalleri, B., Ganguly, J., Perger, W.F., Belmonte, D., and Vetuschi Zuccolini, M. (2010a) Thermo-chemical and thermo-physical properties of the high-pressure phase anhydrous B ($Mg_{14}Si_5O_{24}$): An ab-initio all-electron investigation. American Mineralogist, 95, 563-573.

Ottonello, G., Vetuschi Zuccolini, M., and Belmonte, D. (2010b) The vibrational behaviour of silica clusters at the glass transition: Ab initio calculations and thermodynamic implications. Journal of Chemical Physics, 133, 104508.

Ottonello, G., Attene, M., Ameglio, D., Belmonte, D., Vetuschi Zuccolini, M., and Natali, M. (2013) Thermodynamic investigation of the CaO-Al_2O_3-SiO_2 system at high P and T through polymer chemistry and convex-hull techniques. Chemical Geology, 346, 81-92.

Palko, J.W., Sayir, A., Sinogeikin, S.V., Kriver, W.M., and Bass, J.D. (2002) Complete elastic tensor for mullite (~$2.5Al_2O_3 \cdot SiO_2$) to high temperatures measured from textured fibers. Journal of the American Ceramic Society, 85, 2005-2012.

729 Pascale, F., Zicovich-Wilson, C.M., Lopez-Gejo, F., Civalleri, B., Orlando, R., and Dovesi, R.
730 (2004) The calculation of the vibrational frequencies of crystalline compounds and its
731 implementation in the CRYSTAL code. Journal of Computational Chemistry, 25, 888-897.

732 Perger, W.F., Criswell, J., Civalleri, B., and Dovesi, R. (2009) Ab-initio calculation of elastic
733 constants of crystalline systems with the CRYSTAL code. Computer Physics
734 Communications, 180, 1753-1759.

735 Podlesskii, K.K. (2010) Stability of sapphirine-bearing mineral assemblages in the system FeO-
736 MgO-Al_2O_3-SiO_2 and metamorphic P-T parameters of aluminous granulites. Petrology, 18,
737 350-368.

738 Podlesskii, K.K., Aranovich, L.Y., Gerya, T.V., and Kosyakova, N.A. (2008) Sapphirine-bearing
739 assemblages in the system MgO-Al_2O_3-SiO_2: a continuing ambiguity. European Journal of
740 Mineralogy, 20, 721-734.

741 Prencipe, M., Scanavino, I., Nestola, F., Merlini, M., Civalleri, B., Bruno, M., and Dovesi, R.
742 (2011) High-pressure thermo-elastic properties of beryl ($Al_4Be_6Si_{12}O_{36}$) from ab initio
743 calculations, and observations about the source of thermal expansion. Physics and Chemistry
744 of Minerals, 38, 223-239.

745 Prencipe, M., Mantovani, L., Tribaudino, M., Bersani, D. and Lottici P.P. (2012) The Raman
746 spectrum of diopside: a comparison between *ab initio* calculated and experimentally
747 measured frequencies. European Journal of Mineralogy, 24, 457-464.

748 Richet, P., Bottinga, Y., Deniélou, L., Petitet, J.P., and Téqui, C. (1982) Thermodynamic properties
749 of quartz, cristobalite and amorphous SiO_2: drop calorimetry measurements between 1000
750 and 1800 K and a review from 0 to 2000 K. Geochimica et Cosmochimica Acta, 46, 2639-
751 2658.

752 Robie, R.A., and Hemingway, B.S. (1995) Thermodynamic properties of minerals and related
753 substances at 298.15 K and 1 Bar (10^5 Pascals) pressure and at higher temperatures. U.S.
754 Geological Survey Bullettin 2131.
755 Saxena, S.K., Chatterjee, N., Fei, Y., and Shen G., (1993) Thermodynamic Data on Oxydes and
756 Silicates. Springer-Verlag, Berlin.
757 Schneider, H., and Eberhard, E. (1990) Thermal expansion of mullite. Journal of the American
758 Ceramic Society, 73, 2073-2076.
759 Schreyer, W. (1968) A reconaissance study of the system MgO-Al_2O_3-SiO_2-H_2O at pressures
760 between 10 and 25 kb. Carnegie Institute of Washington Year Book, 66, 380-392.
761 Schreyer, W., and Seifert, F. (1969a) High-pressure phases in the system MgO-Al_2O_3-SiO_2-H_2O.
762 American Journal of Science, 267A, 407-443.
763 Schreyer, W., and Seifert, F. (1969b) Compatibility relations of the aluminum silicates in the
764 system MgO-Al_2O_3-SiO_2-H_2O and K_2O-MgO-Al_2O_3-SiO_2-H_2O at high pressures. American
765 Journal of Science, 267, 371-388.
766 Seifert, F. (1974) Stability of sapphirine: a study of the aluminous part of the system MgO-Al_2O_3-
767 SiO_2-H_2O. Journal of Geology, 82, 173-204.
768 Smart, R.M., and Glasser, F.P. (1976) Phase relations of cordierite and sapphirine in the system
769 MgO-Al_2O_3-SiO_2. Journal of Materials Science, 11, 1459-1464.
770 Taylor, H.C.J. (1973) Melting relations in the system MgO-Al_2O_3-SiO_2 at 15 Kb. Geological
771 Society of America Bulletin, 84, 1335-1348.
772 Többens, D.M., and Kahlenberg, V. (2011) Improved DFT calculation of Raman spectra of
773 silicates. Vibrational Spectroscopy, 56, 265-272.
774 Toohill, K., Siegesmund, S., and Bass, J.D. (1999) Sound velocities and elasticity of cordierite and
775 implications for deep crustal seismic anisotropy. Physics and Chemistry of Minerals, 26,
776 333-343.

777 Ulian, G., Valdrè, G., Corno, M., and Ugliengo, P. (2013) The vibrational features of
778 hydroxylapatite and type A carbonated apatite: a first principle contribution. American
779 Mineralogist, 98, 752-759.

780 Ungureanu, C.G., Cossio, R., and Prencipe, M. (2012) An Ab-initio assessment of thermo-elastic
781 properties of $CaCO_3$ polymorphs: Calcite case. CALPHAD: Computer Coupling of Phase
782 Diagrams and Thermochemistry, 37, 25-33.

783 Whitney, D.L., and Evans, B.W. (2010) Abbreviations for names of rock-forming minerals.
784 American Mineralogist, 95, 185-187.

785

786

787 **FIGURE CAPTIONS**

788

789 **Figure 1**: Pressure-volume curves calculated for sapphirine-442 (open squares) and sapphirine-351
790 (open circles). K_0 and K'_0 are the static bulk modulus and its pressure derivative at T=0 K,
791 respectively.

792

793 **Figure 2**: Comparison between calculated and experimental IR spectra of sapphirine. *Ab initio*
794 results refer to the sapphirine-442 end-member composition ($Mg_4Al_8Si_2O_{20}$). Experimental data of
795 Hofmeister and Bowey (2006) and Christy et al. (1992) refer to natural samples with Si = 1.6 apfu
796 and Si = 1.8 apfu, respectively.

797

798 **Figure 3**: Inverse pole figures of longitudinal seismic velocities (V_P) and quasi-shear wave velocities
799 (V_{S1} and V_{S2}) calculated for (a) sapphirine-442 and (b) sapphirine-351 using the elastic tensors
800 obtained in this study. Single-crystal seismic anisotropies (A_P and A_S, in %) are also reported at the
801 bottom of each stereogram. X1, X2 and X3 are the reference axes, with X1 along [100], X2 along
802 [010] and X3 along [001] crystallographic directions. Contour lines are in Km/s.

803

804 **Figure 4**: Ab initio isobaric heat capacities of sapphirine-442 and sapphirine-351, compared with
805 the experimental data of Kiseleva and Topor (1975). The assessed values of Holland and Powell
806 (2011) are also plotted for comparison. The inset shows the absolute difference between the C_P
807 values calculated for the two sapphirine end-members.

808

809 **Figure 5**: MAS liquidus surface calculated at a) P = 1 bar, b) P = 5 kbar, c) P = 10 kbar and d) P =
810 21 kbar. Abbreviations for minerals as in Whitney and Evans (2010): Trd = tridymite (SiO_2); Crs =
811 cristobalite (SiO_2); Qz-β = quartz-beta (SiO_2); Mul = mullite ($Al_6Si_2O_{13}$); Crd = cordierite
812 ($Mg_2Al_4Si_5O_{18}$); En = enstatite ($MgSiO_3$); Fo = forsterite (Mg_2SiO_4); Spl = spinel ($MgAl_2O_4$); Per =

813 periclase (MgO); Crn = corundum (Al_2O_3); Spr-351 = sapphirine-351 ($Mg_3Al_{10}SiO_{20}$); Spr-442 =

814 sapphirine-442 ($Mg_4Al_8Si_2O_{20}$); Sil = sillimanite (Al_2SiO_5); Prp = pyrope ($Mg_3Al_2Si_3O_{12}$).

Table 1. Site occupancies and structural parameters of the investigated sapphirine-2M end-members ($Mg_4Al_8Si_2O_{20}$ and $Mg_3Al_{10}SiO_{20}$), compared with experimental results.

Site	$\mathbf{Mg_{3.5}Al_{9.0}Si_{1.5}O_{20}}$	$\mathbf{Mg_{3.7}Fe_{0.2}Al_{8.3}Si_{1.8}O_{20}}$	$\mathbf{Mg_{3.15}Fe_{1.05}Al_{8.05}Si_{1.75}O_{20}}$	$\mathbf{Mg_{4.0}Al_{8.0}Si_{2.0}O_{20}}$	$\mathbf{Mg_{3.0}Al_{10.0}Si_{1.0}O_{20}}$
M1	Al	$Mg_{0.04}Al_{0.96}$	$Fe_{0.10}Al_{0.90}$	Al	Al
M2	Al	$Mg_{0.06}Al_{0.94}$	$Fe_{0.10}Al_{0.90}$	Al	Al
M3	$Mg_{0.50}Al_{0.50}$	$Mg_{0.56}Al_{0.44}$	$Mg_{0.70}Fe_{0.30}$	Mg	Al
M4	Mg	Mg	$Mg_{0.85}Fe_{0.15}$	Mg	Mg
M5	Mg	Mg	$Mg_{0.80}Fe_{0.20}$	Mg	Mg
M6	Mg	Mg	$Mg_{0.80}Fe_{0.20}$	Mg	Mg
M7	Al	Al	Al	Al	Al
M8	Al	$Mg_{0.12}Al_{0.88}$	Al	Al	Al
T1	Al	$Si_{0.08}Al_{0.92}$	Al	Al	Al
T2	$Si_{0.75}Al_{0.25}$	$Si_{0.99}Al_{0.01}$	$Si_{0.75}Al_{0.25}$	Si	Si
T3	$Si_{0.50}Al_{0.50}$	$Si_{0.49}Al_{0.51}$	$Si_{0.50}Al_{0.50}$	Si	Al
T4	$Si_{0.25}Al_{0.75}$	$Si_{0.08}Al_{0.92}$	$Si_{0.25}Al_{0.75}$	Al	Al
T5	Al	Al	Al	Al	Al
T6	Al	$Si_{0.27}Al_{0.73}$	$Si_{0.25}Al_{0.75}$	Al	Al
a (Å)	11.266(12)	11.286(3)	11.31(1)	11.363	11.375
b (Å)	14.401(70)	14.438(2)	14.48(1)	14.610	14.461
c (Å)	9.929(10)	9.957(2)	9.99(1)	9.903	9.875
β (°)	125.4(5)	125.4(2)	125.4(2)	124.289	124.285
V_{cell} ($Å^3$)	1311(3)	1322.52	1333.59	1358.4	1342.2
a/*b*	0.7823	0.7817	0.7811	0.7778	0.7866
c/*a*	0.8813	0.8822	0.8833	0.8715	0.8681
Reference	Moore (1969)	Higgins and Ribbe (1979)	Merlino (1980)	this work	this work

Notes: Ab initio results refer to T = 0 K and P = 0, experimental data to ambient conditions (T = 298.15 K and P =1 bar). Experimental data have been obtained by single-crystal X-ray diffraction (Moore 1969; Merlino 1980) or neutron diffraction (Higgins and Ribbe 1979).

822 **Table 2.** Mean bond distances calculated for sapphirine-442 ($Mg_4Al_8Si_2O_{20}$) and sapphirine-351 ($Mg_3Al_{10}SiO_{20}$), in comparison with
823 experimental data.
824

Mean bond distances (Å)	Moore (1969)	Higgins and Ribbe (1979)	Merlino (1980)	Sapphirine-442 (this work)	Sapphirine-351 (this work)
<M1-O>	1.926	1.932	1.94	1.936	1.934
<M2-O>	1.930	1.938	1.94	1.934	1.935
<M3-O>	1.988	2.001	2.02	2.085	1.946
<M4-O>	2.078	2.080	2.10	2.105	2.090
<M5-O>	2.120	2.120	2.13	2.150	2.132
<M6-O>	2.115	2.118	2.13	2.147	2.132
<M7-O>	1.921	1.929	1.92	1.927	1.934
<M8-O>	1.930	1.938	1.94	1.942	1.937
<T1-O>	1.771	1.757	1.78	1.778	1.776
<T2-O>	1.658	1.656	1.66	1.643	1.642
<T3-O>	1.700	1.711	1.70	1.646	1.759
<T4-O>	1.733	1.750	1.73	1.773	1.771
<T5-O>	1.755	1.758	1.78	1.787	1.790
<T6-O>	1.736	1.735	1.73	1.788	1.787

825
826
827 **Table 3.** Ab initio axial and volume compression data of sapphirine-442 ($Mg_4Al_8Si_2O_{20}$) and sapphirine-351 ($Mg_3Al_{10}SiO_{20}$),
828 calculated in the pressure range P = 0 ÷ 10 GPa.
829

	Sapphirine-442					Sapphirine-351				
P (GPa)	a/a_0	b/b_0	c/c_0	β (°)	V/V_0	a/a_0	b/b_0	c/c_0	β (°)	V/V_0
0.0	1.0000	1.0000	1.0000	124.289	1.0000	1.0000	1.0000	1.0000	124.285	1.0000
0.5	0.9990	0.9989	0.9989	124.275	0.9969	0.9990	0.9990	0.9990	124.277	0.9971
1.0	0.9980	0.9978	0.9978	124.264	0.9939	0.9980	0.9981	0.9980	124.268	0.9943
1.5	0.9970	0.9966	0.9967	124.250	0.9908	0.9971	0.9971	0.9970	124.261	0.9915
2.0	0.9961	0.9955	0.9957	124.239	0.9879	0.9961	0.9962	0.9960	124.248	0.9888
3.0	0.9942	0.9934	0.9936	124.216	0.9821	0.9942	0.9944	0.9941	124.235	0.9834
4.0	0.9924	0.9913	0.9916	124.200	0.9766	0.9924	0.9925	0.9923	124.222	0.9780
5.0	0.9905	0.9892	0.9896	124.176	0.9710	0.9905	0.9909	0.9904	124.203	0.9731
7.0	0.9871	0.9853	0.9859	124.143	0.9605	0.9871	0.9874	0.9869	124.177	0.9631
10.0	0.9822	0.9801	0.9808	124.100	0.9463	0.9820	0.9828	0.9819	124.135	0.9494

830

831 **Table 4.** Ab initio B3LYP stiffnesses (c_{ij}) and compliances (s_{ij}) calculated for sapphirine-442 ($Mg_4Al_8Si_2O_{20}$) and sapphirine-351
832 ($Mg_3Al_{10}SiO_{20}$).
833

Sapphirine-442				Sapphirine-351			
c_{ij} (GPa)		s_{ij} $(GPa)^{-1}$		c_{ij} (GPa)		s_{ij} $(GPa)^{-1}$	
c_{11}	300.86	s_{11}	398.02×10^{-5}	c_{11}	302.78	s_{11}	411.93×10^{-5}
c_{22}	300.91	s_{22}	390.27×10^{-5}	c_{22}	333.89	s_{22}	359.56×10^{-5}
c_{33}	336.66	s_{33}	329.88×10^{-5}	c_{33}	360.38	s_{33}	309.31×10^{-5}
c_{44}	86.62	s_{44}	1267.95×10^{-5}	c_{44}	91.16	s_{44}	1194.06×10^{-5}
c_{55}	98.86	s_{55}	1061.60×10^{-5}	c_{55}	105.53	s_{55}	1002.42×10^{-5}
c_{66}	109.34	s_{66}	1004.53×10^{-5}	c_{66}	124.73	s_{66}	872.74×10^{-5}
c_{12}	94.35	s_{12}	-114.02×10^{-5}	c_{12}	111.39	s_{12}	-127.79×10^{-5}
c_{13}	91.41	s_{13}	-87.44×10^{-5}	c_{13}	95.55	s_{13}	-86.69×10^{-5}
c_{23}	66.65	s_{23}	-43.46×10^{-5}	c_{23}	74.25	s_{23}	-36.53×10^{-5}
c_{15}	–11.45	s_{15}	87.04×10^{-5}	c_{15}	–18.89	s_{15}	116.76×10^{-5}
c_{25}	29.73	s_{25}	-127.26×10^{-5}	c_{25}	27.56	s_{25}	-112.72×10^{-5}
c_{35}	7.52	s_{35}	-22.15×10^{-5}	c_{35}	11.73	s_{35}	-40.37×10^{-5}
c_{46}	29.12	s_{46}	-337.72×10^{-5}	c_{46}	30.41	s_{46}	-291.12×10^{-5}

Table 5. Ab initio single-crystal, directionally averaged and aggregate seismic properties of sapphirine-442 ($Mg_4Al_8Si_2O_{20}$) and sapphirine-351 ($Mg_3Al_{10}SiO_{20}$).

Sapphirine-442		Sapphirine-351	
$V_{S,MIN}$ (Km/s)	4.45	$V_{S,MIN}$ (Km/s)	4.63
$V_{S,MAX}$ (Km/s)	6.21	$V_{S,MAX}$ (Km/s)	6.46
u_1 (Km/s)	5.21	u_1 (Km/s)	5.32
u_2 (Km/s)	5.79	u_2 (Km/s)	5.98
u_3 (Km/s)	9.34	u_3 (Km/s)	9.62
$V_{S,VRH}$ (Km/s)	5.47	$V_{S,VRH}$ (Km/s)	5.61
$V_{P,VRH}$ (Km/s)	9.34	$V_{P,VRH}$ (Km/s)	9.62
K_V (GPa)	160.36	K_V (GPa)	173.27
K_R (GPa)	159.16	K_R (GPa)	172.78
K_{VRH} (GPa)	159.76	K_{VRH} (GPa)	173.02
μ_V (GPa)	104.70	μ_V (GPa)	112.01
μ_R (GPa)	97.06	μ_R (GPa)	103.20
μ_{VRH} (GPa)	100.88	μ_{VRH} (GPa)	107.60
E (GPa)	249.97	E (GPa)	267.32
ν_P	0.239	ν_P	0.243
ρ_0 (g/cm^3)	3.370	ρ_0 (g/cm^3)	3.419

Notes: $V_{S,MIN}$, $V_{S,MAX}$ = single-crystal slowest and fastest shear-wave velocities; u_1, u_2 = directionally averaged shear-wave velocities, u_3 = directionally averaged longitudinal-wave velocity; $V_{S,VRH}$, $V_{P,VRH}$ = Voigt-Reuss-Hill aggregate shear and longitudinal seismic velocities; K_V, K_R, K_{VRH} = Voigt, Reuss and Voigt-Reuss-Hill bulk moduli; μ_V, μ_R, $_{KVRH}$ = Voigt, Reuss and Voigt-Reuss-Hill shear moduli; E = Young's modulus; ν_P = Poisson's ratio; ρ_0 = density at the athermal limit (i.e. P = 0 GPa and T=0K).

Table 6. Thermochemical reference data for the atoms of interest in this study.

Species	$H^0_{f,Ai,0}$ (kJ/mol)	$\Delta H_{element,i,0\rightarrow298.15}$ (kJ/mol)	E_{Ai} (hartree)
Si	445.668	3.2180	–289.293670
O	246.790	4.3415	–75.057906
Mg	145.900	4.9980	–200.014400
Al	327.300	4.5390	–242.283402

Notes: $H^0_{f,0}$ = enthalpy of formation of the gaseous atom from the stable element at T = 0 K, P = 1 bar (NIST-JANAF Tables; Chase 1998). $\Delta H_{element,i,0\rightarrow298.15}$ is the enthalpy difference between T = 298. 15 K and T = 0 K for the monoatomic element (NIST-JANAF Tables; Chase 1998). E_{Ai} is the electronic energies of the gaseous atoms yielding a correct heat content of the constituent oxides at standard state in the compositional system MgO-Al_2O_3-SiO_2: the results obtained by Robie and Hemingway (1995) for periclase, Ditmars et al. (1982) for corundum and Richet et al. (1982) for quartz-α are taken as reference values (see Table 7).

Table 7. Thermochemical data for heat content calculation of sapphirine-442 ($Mg_4Al_8Si_2O_{20}$) and sapphirine-321 ($Mg_3Al_{10}SiO_{20}$).

Substance	D_0 (kJ/mol)	$E_{0,crystal}$ (hartree)	$E_{ZPE,crystal}$ (kJ/mol)	$H_{vib,298.15}$ (kJ/mol)	$H^0_{f,298.15}$ / B3LYP (kJ/mol)	$H°_{f,298.15}$ / Expt. (kJ/mol)	Ref.
MgO (periclase)	989.8	–275.454828	14.5	19.5	–601.4	–601.6	1, 2
α-Al_2O_3 (corundum)	3058.7	–710.922481	44.6	54.6	–1675.7	–1675.7 ± 1.2	3, 4
α-SiO_2 (quartz)	1845.0	–440.123389	29.4	36.3	–910.7	–910.7	5, 6
α-Mg_2SiO_4 (forsterite)	3883.4	–991.055720	59.1	75.7	–2172.7	–2173.0	1, 2
$Mg_4Al_8Si_2O_{20}$ (sapphirine-442)	20113.5	–4825.844937	298.7	374.6	–11158.0 (–11088.0)[a]	–11005 ± 33.5[b]	7
$Mg_3Al_{10}SiO_{20}$ (sapphirine-351)	20351.7	–4821.194682	299.5	374.1	–11335.3 (–11203.3)[a]	–11106 ± 8.0[c]	7

Notes: (1) this work; (2) Robie and Hemingway (1995); (3) Ditmars et al. (1982) ; (4) NIST-JANAF Tables (Chase 1998); (5) Ottonello et al., (2009b); (6) Richet et al. (1982); (7) Kiseleva (1976). [a] Optimized value according to MAS phase topology (see text for details). [b] Value measured on a synthetic disordered sample of formula $Mg_4Al_8Si_2O_{20}$. [c] Value measured on a natural ordered sample of formula $Mg_{3.5}Al_{9.0}Si_{1.5}O_{20}$.

Table 8. Ab initio B3LYP thermodynamic and thermophysical data for sapphirine-442 ($Mg_4Al_8Si_2O_{20}$) and sapphirine-351 ($Mg_3Al_{10}SiO_{20}$).

	Sapphirine-442	Sapphirine-351
V^0_{298} (cc/mol)	204.879	202.387
S^0_{298} (J/mol×K)	407.0	397.6
$\Delta_f H^0_{298}$ (kJ/mol)	–11088.0	–11203.3
K_0 (GPa)	158.73	172.33
K'_0	4.68	4.28
$(dK/dT)_P$ (bar/K)	–210.2	–188.0
$\alpha_0 \times 10^9$	9.0302	6.0817
$\alpha_1 \times 10^5$	1.0411	1.5709
$\alpha_2 \times 10^3$	14.0340	8.2836
α_3	–6.4469	–4.3554
α_4	814.288	547.232
a	791.61	789.73
$b \times 10^3$	65.455	60.300
$c \times 10^{-5}$	–181.750	–91.751
d	–481.63	–782.10
$e \times 10^{-8}$	–9.1576	–31.847
$f \times 10^6$	3.4196	13.270
$g \times 10^9$	–2.0517	–5.1473

Notes: V^0_{298} = molar volume at standard state (T=298.15 K and P = 1bar); S^0_{298} = standard state entropy; $\Delta_f H°_{298}$ = enthalpy of formation from the elements at standard state; K_0 = static bulk modulus; K'_0 = pressure derivative of bulk modulus; $(dK/dT)_P$ = isobaric temperature derivative of bulk modulus; α_0, α_1, α_2, α_3, α_4 = numerical coefficients of the polynomial function for thermal expansion (see Eq. 18); a, b, c, d, e, f, g = numerical coefficients of the polynomial function for isobaric heat capacity (C_P) (see Eq. 21).

914 **Table 9.** Standard state thermodynamic properties of sapphirine end-members at 1 bar, 298.15 K.
915

$Mg_4Al_8Si_2O_{20}$ (sapphirine-442)	$\Delta_fH^0_{298}$ (kJ/mol)	S^0_{298} (J/mol×K)	V^0_{298} (cc/mol)
this work	–11088.028	406.975	204.879
Kiseleva (1976)	–11005.6 ± 33.5	411.7056	-
Holland & Powell (1998)	–11014.08	440.00	198.70
Logvinkov et al. (2001)	–11107.497	390.34172	-
Kelsey et al. (2004)	–11003.38	450.00	199.05
Podlesskii et al. (2008)	–11018.469[a] (–11003.035)[b]	413.75[a] (425.32)[b]	198.61[a] (198.61)[b]
Holland & Powell (2011)	–11022.40	425.50	199.00
$Mg_3Al_{10}SiO_{20}$ (sapphirine-351)	$\Delta_fH^0_{298}$ (kJ/mol)	S^0_{298} (J/mol×K)	V^0_{298} (cc/mol)
this work	–11203.294	397.575	202.387
Kelsey et al. (2004)	–11138.46	420.00	197.51
Podlesskii et al. (2008)	–11168.243[a] (–11181.724)[b]	379.67[a] (367.94)[b]	196.67[a] (196.51)[b]
Holland & Powell (2011)	–11135.69	419.50	197.50

916
917 *Notes:* V^0_{298} = molar volume at standard state (T=298.15 K and P = 1bar); S^0_{298} = standard state
918 entropy; $\Delta_fH°_{298}$ = enthalpy of formation from the elements at standard state; a = end-member
919 properties for the ideal solid solution; b = end-member properties for the non-ideal solid solution.
920
921
922
923

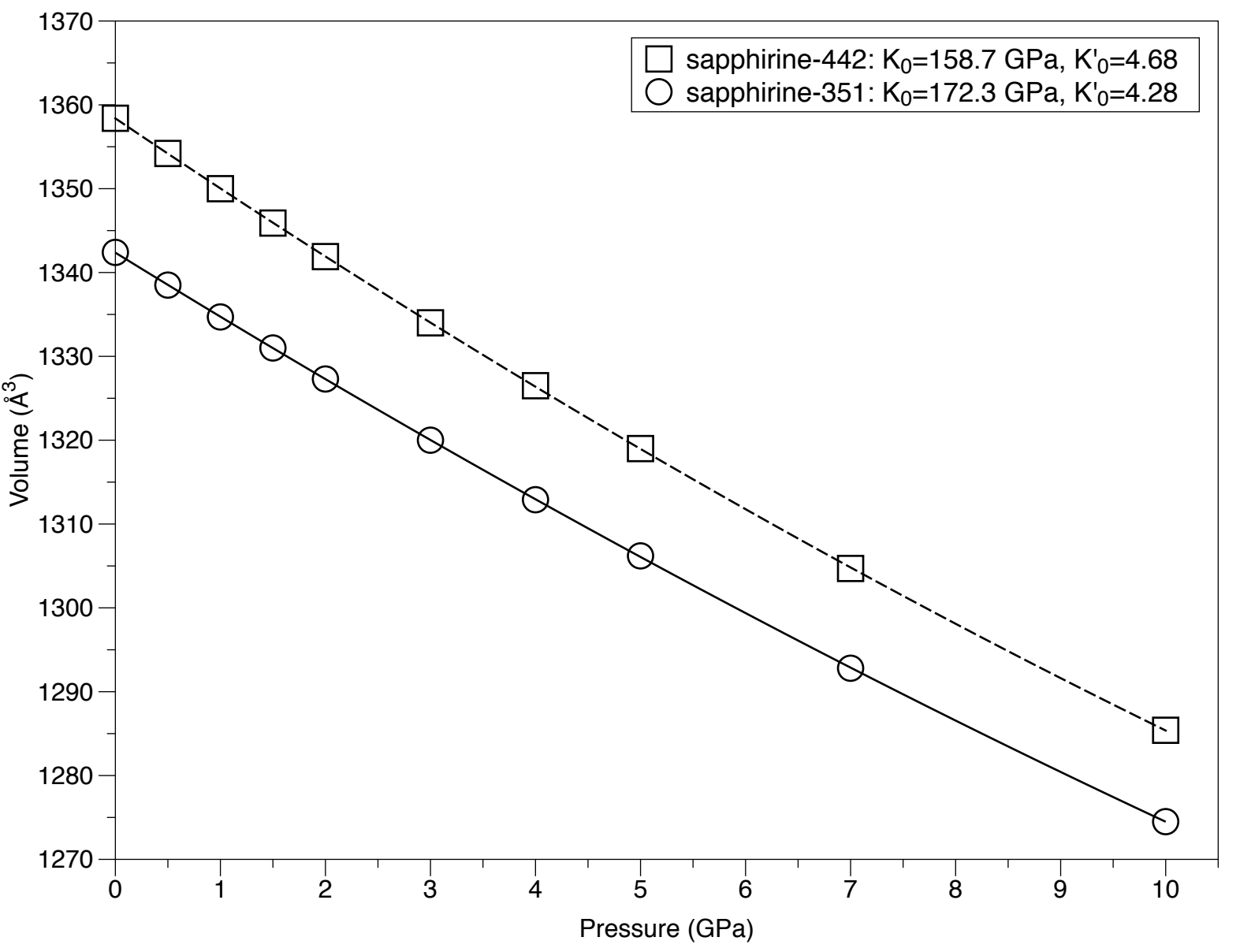
sapphirine-442: K0=158.7 GPa, K'0=4.68
sapphirine-351: K0=172.3 GPa, K'0=4.28
Volume (Å3)
Pressure (GPa)
1370
1360
1350
1340
1330
1320
1310
1300
1290
1280
1270
0
1
2
3
4
5
6
7
8
9
10

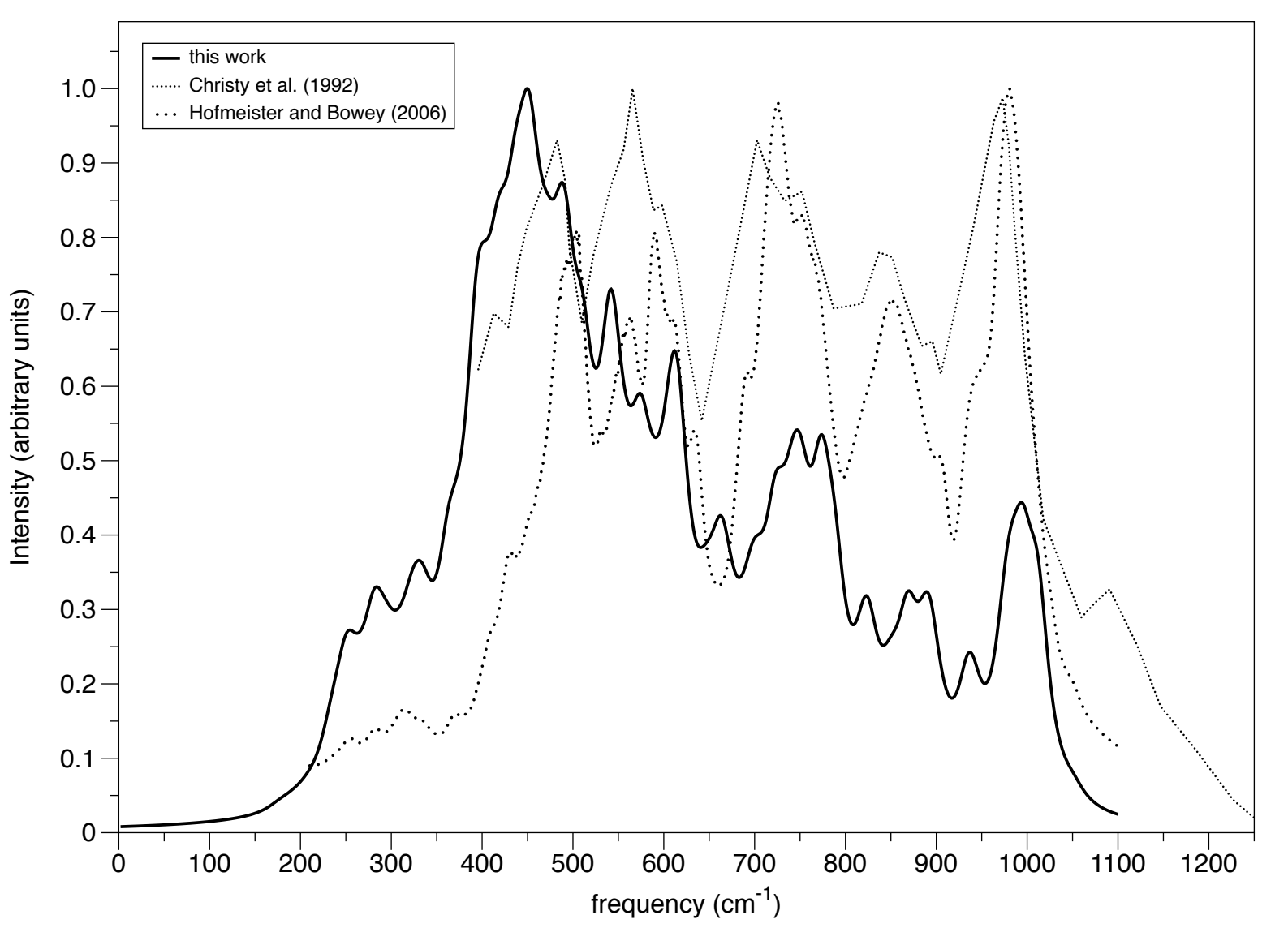
this work
Christy et al. (1992)
Hofmeister and Bowey (2006)
Intensity (arbitrary units)
frequency (cm-1)
0
0.1
0.2
0.3
0.4
0.5
0.6
0.7
0.8
0.9
1.0
0
100
200
300
400
500
600
700
800
900
1000
1100
1200

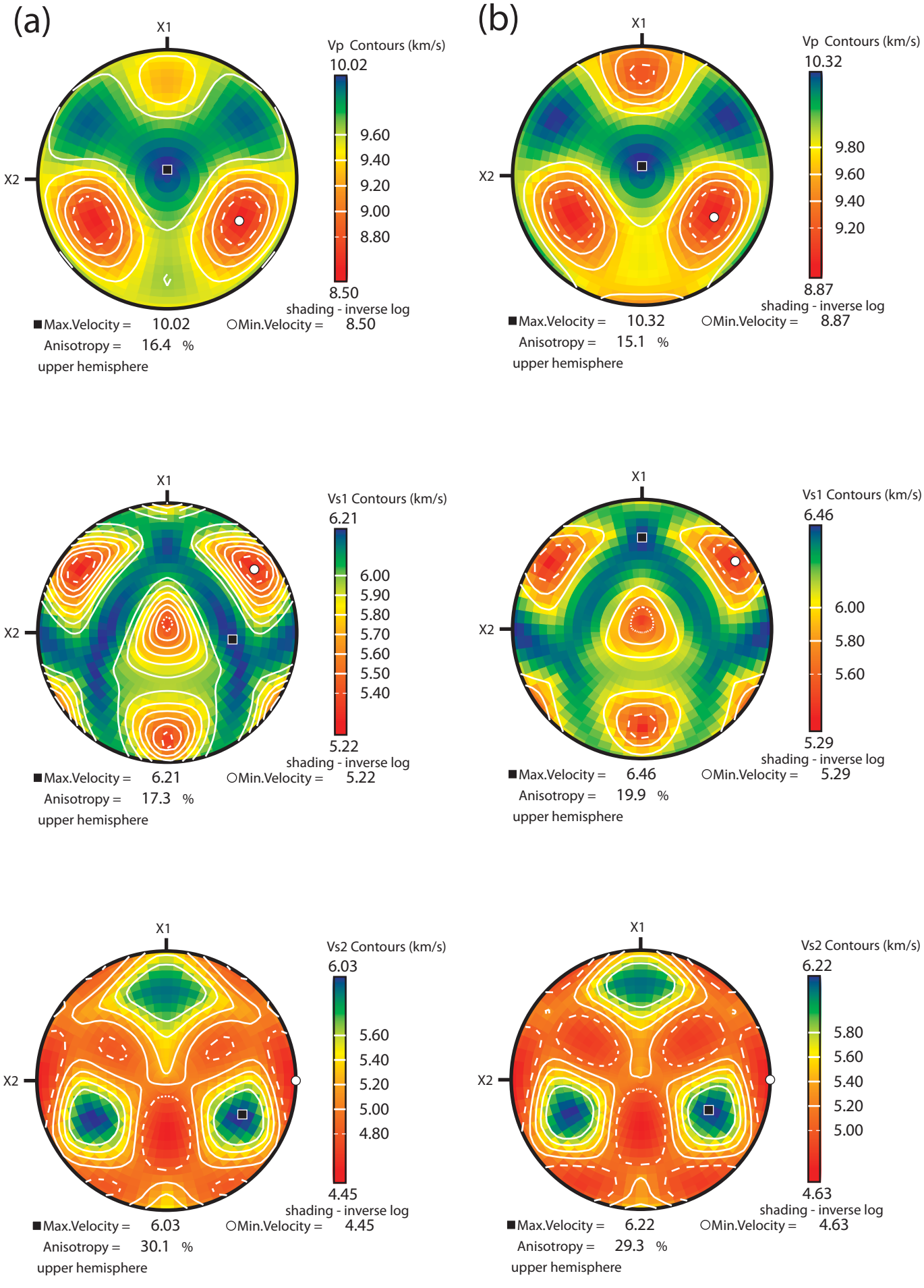
(a)
X1
X2
Vp Contours (km/s)
10.02
9.60
9.40
9.20
9.00
8.80
8.50
shading - inverse log
Max.Velocity = 10.02
Min.Velocity = 8.50
Anisotropy = 16.4 %
upper hemisphere
(b)
X1
X2
Vp Contours (km/s)
10.32
9.80
9.60
9.40
9.20
8.87
shading - inverse log
Max.Velocity = 10.32
Min.Velocity = 8.87
Anisotropy = 15.1 %
upper hemisphere
X1
X2
Vs1 Contours (km/s)
6.21
6.00
5.90
5.80
5.70
5.60
5.50
5.40
5.22
shading - inverse log
Max.Velocity = 6.21
Min.Velocity = 5.22
Anisotropy = 17.3 %
upper hemisphere
X1
X2
Vs1 Contours (km/s)
6.46
6.00
5.80
5.60
5.29
shading - inverse log
Max.Velocity = 6.46
Min.Velocity = 5.29
Anisotropy = 19.9 %
upper hemisphere
X1
X2
Vs2 Contours (km/s)
6.03
5.60
5.40
5.20
5.00
4.80
4.45
shading - inverse log
Max.Velocity = 6.03
Min.Velocity = 4.45
Anisotropy = 30.1 %
upper hemisphere
X1
X2
Vs2 Contours (km/s)
6.22
5.80
5.60
5.40
5.20
5.00
4.63
shading - inverse log
Max.Velocity = 6.22
Min.Velocity = 4.63
Anisotropy = 29.3 %
upper hemisphere

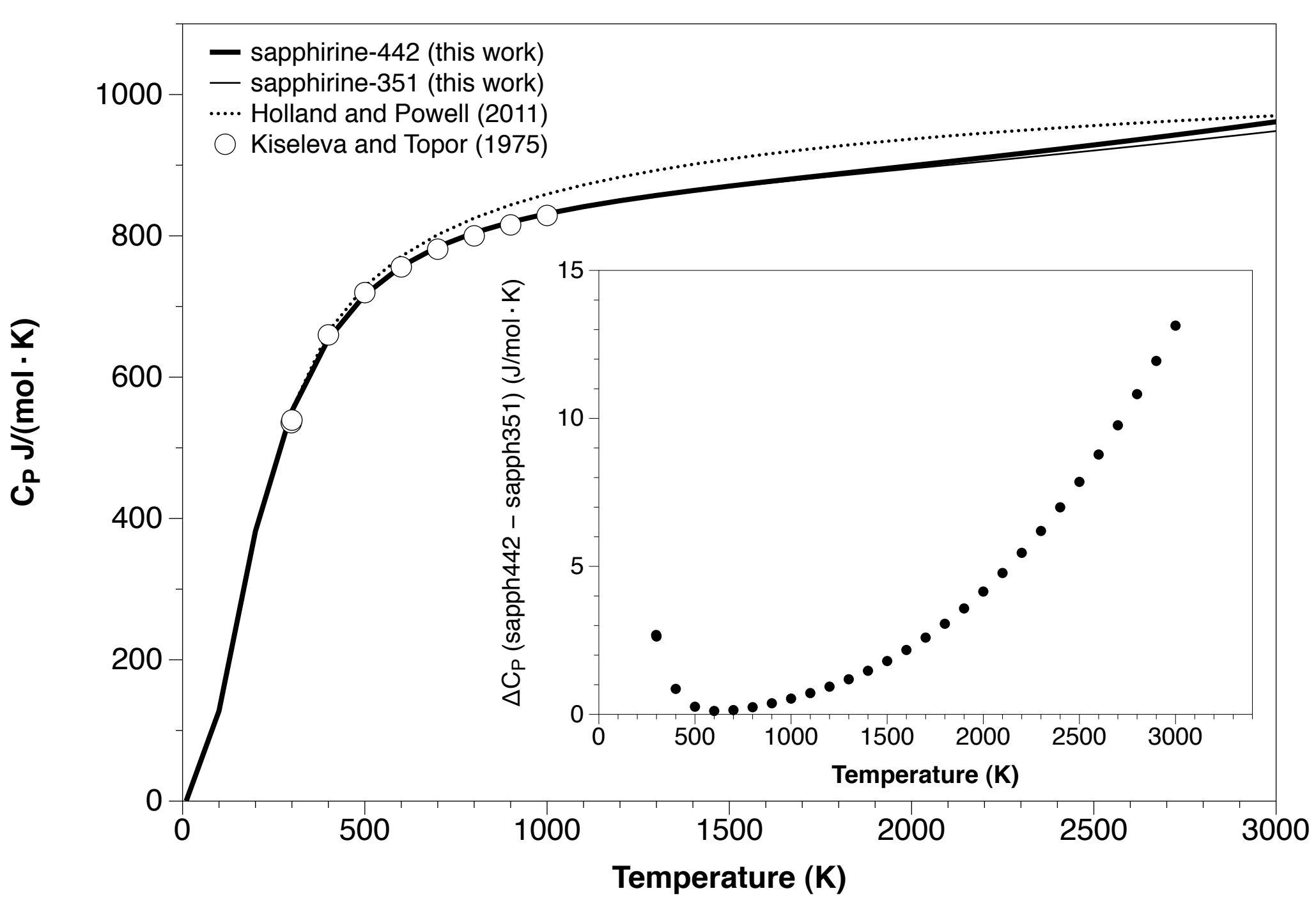
sapphirine-442 (this work)
sapphirine-351 (this work)
Holland and Powell (2011)
Kiseleva and Topor (1975)
C_P J/(mol · K)
Temperature (K)
0
200
400
600
800
1000
0
500
1000
1500
2000
2500
3000
ΔC_P (sapph442 – sapph351) (J/mol · K)
0
5
10
15
0
500
1000
1500
2000
2500
3000
Temperature (K)

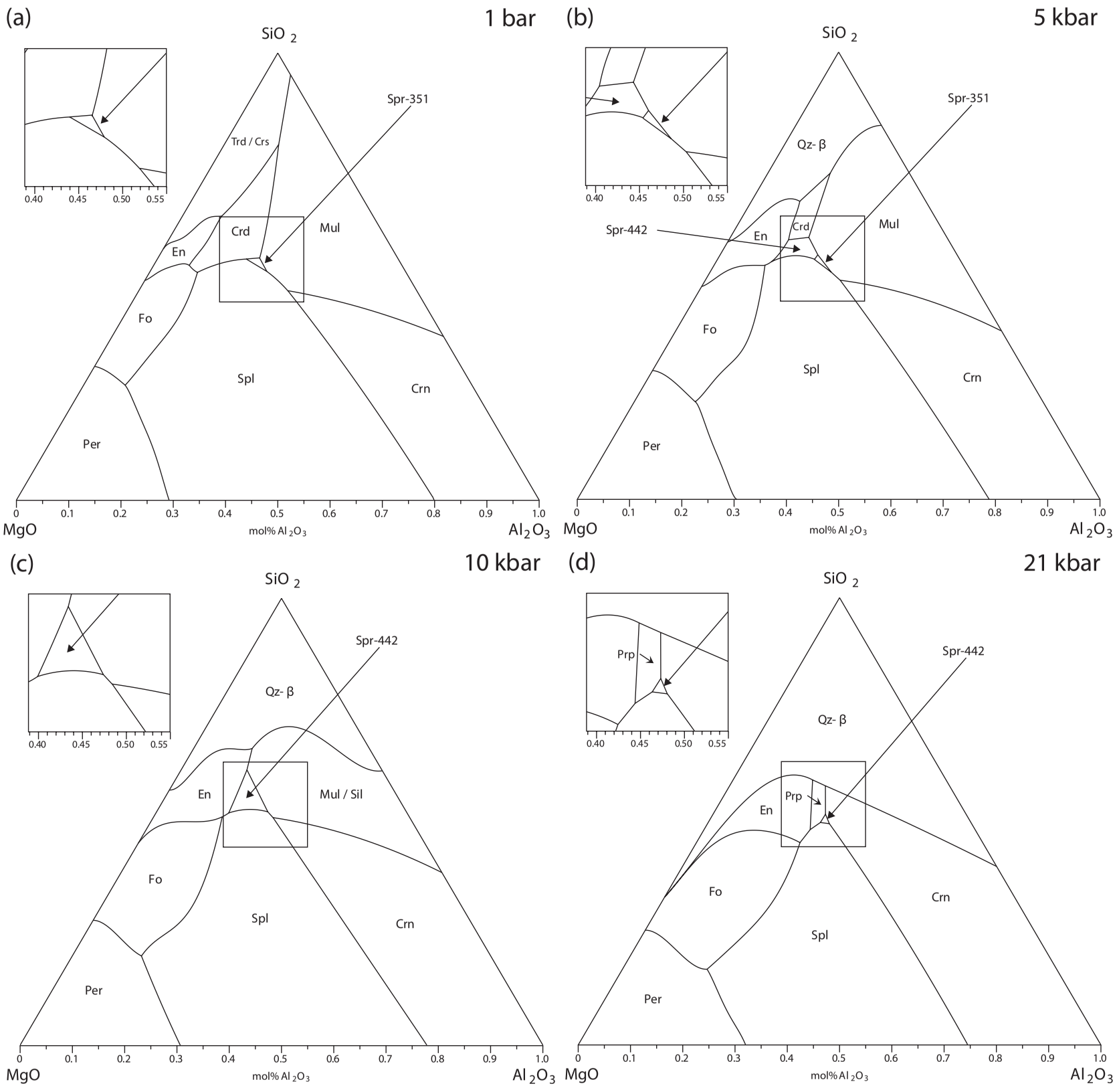
(a)
1 bar
SiO 2
Spr-351
Trd / Crs
Crd
Mul
En
Fo
Spl
Crn
Per
0.40 0.45 0.50 0.55
0 0.1 0.2 0.3 0.4 0.5 0.6 0.7 0.8 0.9 1.0
MgO
mol% Al 2O3
Al2O3
(b)
5 kbar
SiO 2
Spr-351
Qz- β
Spr-442
En
Crd
Mul
Fo
Spl
Crn
Per
0.40 0.45 0.50 0.55
0 0.1 0.2 0.3 0.4 0.5 0.6 0.7 0.8 0.9 1.0
MgO
mol% Al 2O3
Al2O3
(c)
10 kbar
SiO 2
Spr-442
Qz- β
En
Mul / Sil
Fo
Spl
Crn
Per
0.40 0.45 0.50 0.55
0 0.1 0.2 0.3 0.4 0.5 0.6 0.7 0.8 0.9 1.0
MgO
mol% Al 2O3
Al2O3
(d)
21 kbar
SiO 2
Prp
Spr-442
Qz- β
En
Prp
Fo
Crn
Spl
Per
0.40 0.45 0.50 0.55
0 0.1 0.2 0.3 0.4 0.5 0.6 0.7 0.8 0.9 1.0
MgO
mol% Al 2O3
Al2O3

Table 1. Site occupancies and structural parameters of the investigated sapphirine-2M end-members ($Mg_4Al_8Si_2O_{20}$ and $Mg_3Al_{10}SiO_{20}$), compared with experimental results.

Site	$\mathbf{Mg_{3.5}Al_{9.0}Si_{1.5}O_{20}}$	$\mathbf{Mg_{3.7}Fe_{0.2}Al_{8.3}Si_{1.8}O_{20}}$	$\mathbf{Mg_{3.15}Fe_{1.05}Al_{8.05}Si_{1.75}O_{20}}$	$\mathbf{Mg_{4.0}Al_{8.0}Si_{2.0}O_{20}}$	$\mathbf{Mg_{3.0}Al_{10.0}Si_{1.0}O_{20}}$
M1	Al	$Mg_{0.04}Al_{0.96}$	$Fe_{0.10}Al_{0.90}$	Al	Al
M2	Al	$Mg_{0.06}Al_{0.94}$	$Fe_{0.10}Al_{0.90}$	Al	Al
M3	$Mg_{0.50}Al_{0.50}$	$Mg_{0.56}Al_{0.44}$	$Mg_{0.70}Fe_{0.30}$	Mg	Al
M4	Mg	Mg	$Mg_{0.85}Fe_{0.15}$	Mg	Mg
M5	Mg	Mg	$Mg_{0.80}Fe_{0.20}$	Mg	Mg
M6	Mg	Mg	$Mg_{0.80}Fe_{0.20}$	Mg	Mg
M7	Al	Al	Al	Al	Al
M8	Al	$Mg_{0.12}Al_{0.88}$	Al	Al	Al
T1	Al	$Si_{0.08}Al_{0.92}$	Al	Al	Al
T2	$Si_{0.75}Al_{0.25}$	$Si_{0.99}Al_{0.01}$	$Si_{0.75}Al_{0.25}$	Si	Si
T3	$Si_{0.50}Al_{0.50}$	$Si_{0.49}Al_{0.51}$	$Si_{0.50}Al_{0.50}$	Si	Al
T4	$Si_{0.25}Al_{0.75}$	$Si_{0.08}Al_{0.92}$	$Si_{0.25}Al_{0.75}$	Al	Al
T5	Al	Al	Al	Al	Al
T6	Al	$Si_{0.27}Al_{0.73}$	$Si_{0.25}Al_{0.75}$	Al	Al
a (Å)	11.266(12)	11.286(3)	11.31(1)	11.363	11.375
b (Å)	14.401(70)	14.438(2)	14.48(1)	14.610	14.461
c (Å)	9.929(10)	9.957(2)	9.99(1)	9.903	9.875
β (°)	125.4(5)	125.4(2)	125.4(2)	124.289	124.285
V_{cell} (Å^3)	1311(3)	1322.52	1333.59	1358.4	1342.2
a/*b*	0.7823	0.7817	0.7811	0.7778	0.7866
c/*a*	0.8813	0.8822	0.8833	0.8715	0.8681
Reference	Moore (1969)	Higgins and Ribbe (1979)	Merlino (1980)	this work	this work

Notes: Ab initio results refer to T = 0 K and P = 0, experimental data to ambient conditions (T = 298.15 K and P =1 bar). Experimental data have been obtained by single-crystal X-ray diffraction (Moore 1969; Merlino 1980) or neutron diffraction (Higgins and Ribbe 1979).

Table 2. Mean bond distances calculated for sapphirine-442 ($Mg_4Al_8Si_2O_{20}$) and sapphirine-351 ($Mg_3Al_{10}SiO_{20}$), in comparison with experimental data. Values in parenthesis are the deviations of experimental mean bond distances from calculated results for sapphirine-442 (round brackets) and sapphirine-351 (square brackets).

Mean bond distances (Å)	Moore (1969)	Higgins and Ribbe (1979)	Merlino (1980)	Sapphirine-442 (this work)	Sapphirine-351 (this work)
<M1-O>	1.926 (-0.010) [-0.008]	1.932 (-0.004) [-0.002]	1.94 (0.00) [+0.01]	1.936	1.934
<M2-O>	1.930 (-0.004) [-0.005]	1.938 (+0.004) [+0.003]	1.94 (+0.01) [0.00]	1.934	1.935
<M3-O>	1.988 (-0.097) [+0.042]	2.001 (-0.084) [+0.055]	2.02 (-0.06) [+0.07]	2.085	1.946
<M4-O>	2.078 (-0.027) [-0.012]	2.080 (-0.025) [-0.010]	2.10 (0.00) [+0.01]	2.105	2.090
<M5-O>	2.120 (-0.030) [-0.012]	2.120 (-0.030) [-0.012]	2.13 (-0.02) [0.00]	2.150	2.132
<M6-O>	2.115 (-0.032) [-0.017]	2.118 (-0.029) [-0.014]	2.13 (-0.02) [0.00]	2.147	2.132
<M7-O>	1.921 (-0.006) [-0.013]	1.929 (+0.002) [-0.005]	1.92 (-0.01) [-0.01]	1.927	1.934
<M8-O>	1.930 (-0.012) [-0.007]	1.938 (-0.004) [+0.001]	1.94 (0.00) [0.00]	1.942	1.937
<T1-O>	1.771 (-0.007) [-0.005]	1.757 (-0.021) [-0.019]	1.78 (0.00) [0.00]	1.778	1.776
<T2-O>	1.658 (+0.015) [+0.016]	1.656 (+0.013) [+0.014]	1.66 (+0.02) [+0.02]	1.643	1.642
<T3-O>	1.700 (+0.054) [-0.059]	1.711 (+0.065) [-0.048]	1.70 (+0.05) [-0.06]	1.646	1.759
<T4-O>	1.733 (-0.040) [-0.038]	1.750 (-0.023) [-0.021]	1.73 (-0.04) [-0.04]	1.773	1.771
<T5-O>	1.755 (-0.032) [-0.035]	1.758 (-0.029) [-0.032]	1.78 (-0.01) [-0.01]	1.787	1.790
<T6-O>	1.736 (-0.052) [-0.051]	1.735 (-0.053) [-0.052]	1.73 (-0.06) [-0.06]	1.788	1.787

Table 3. Ab initio axial and volume compression data of sapphirine-442 ($Mg_4Al_8Si_2O_{20}$) and sapphirine-351 ($Mg_3Al_{10}SiO_{20}$), calculated in the pressure range P = 0 ÷ 10 GPa.

	Sapphirine-442					Sapphirine-351				
P (GPa)	a/a_0	b/b_0	c/c_0	β (°)	V/V_0	a/a_0	b/b_0	c/c_0	β (°)	V/V_0
0.0	1.0000	1.0000	1.0000	124.289	1.0000	1.0000	1.0000	1.0000	124.285	1.0000
0.5	0.9990	0.9989	0.9989	124.275	0.9969	0.9990	0.9990	0.9990	124.277	0.9971
1.0	0.9980	0.9978	0.9978	124.264	0.9939	0.9980	0.9981	0.9980	124.268	0.9943
1.5	0.9970	0.9966	0.9967	124.250	0.9908	0.9971	0.9971	0.9970	124.261	0.9915
2.0	0.9961	0.9955	0.9957	124.239	0.9879	0.9961	0.9962	0.9960	124.248	0.9888
3.0	0.9942	0.9934	0.9936	124.216	0.9821	0.9942	0.9944	0.9941	124.235	0.9834
4.0	0.9924	0.9913	0.9916	124.200	0.9766	0.9924	0.9925	0.9923	124.222	0.9780
5.0	0.9905	0.9892	0.9896	124.176	0.9710	0.9905	0.9909	0.9904	124.203	0.9731
7.0	0.9871	0.9853	0.9859	124.143	0.9605	0.9871	0.9874	0.9869	124.177	0.9631
10.0	0.9822	0.9801	0.9808	124.100	0.9463	0.9820	0.9828	0.9819	124.135	0.9494

Table 4. Ab initio B3LYP stiffnesses (c_{ij}) and compliances (s_{ij}) calculated for sapphirine-442 ($Mg_4Al_8Si_2O_{20}$) and sapphirine-351 ($Mg_3Al_{10}SiO_{20}$).

Sapphirine-442				Sapphirine-351			
c_{ij} (GPa)		s_{ij} $(GPa)^{-1}$		c_{ij} (GPa)		s_{ij} $(GPa)^{-1}$	
c_{11}	300.86	s_{11}	398.02×10^{-5}	c_{11}	302.78	s_{11}	411.93×10^{-5}
c_{22}	300.91	s_{22}	390.27×10^{-5}	c_{22}	333.89	s_{22}	359.56×10^{-5}
c_{33}	336.66	s_{33}	329.88×10^{-5}	c_{33}	360.38	s_{33}	309.31×10^{-5}
c_{44}	86.62	s_{44}	1267.95×10^{-5}	c_{44}	91.16	s_{44}	1194.06×10^{-5}
c_{55}	98.86	s_{55}	1061.60×10^{-5}	c_{55}	105.53	s_{55}	1002.42×10^{-5}
c_{66}	109.34	s_{66}	1004.53×10^{-5}	c_{66}	124.73	s_{66}	872.74×10^{-5}
c_{12}	94.35	s_{12}	-114.02×10^{-5}	c_{12}	111.39	s_{12}	-127.79×10^{-5}
c_{13}	91.41	s_{13}	-87.44×10^{-5}	c_{13}	95.55	s_{13}	-86.69×10^{-5}
c_{23}	66.65	s_{23}	-43.46×10^{-5}	c_{23}	74.25	s_{23}	-36.53×10^{-5}
c_{15}	–11.45	s_{15}	87.04×10^{-5}	c_{15}	–18.89	s_{15}	116.76×10^{-5}
c_{25}	29.73	s_{25}	-127.26×10^{-5}	c_{25}	27.56	s_{25}	-112.72×10^{-5}
c_{35}	7.52	s_{35}	-22.15×10^{-5}	c_{35}	11.73	s_{35}	-40.37×10^{-5}
c_{46}	29.12	s_{46}	-337.72×10^{-5}	c_{46}	30.41	s_{46}	-291.12×10^{-5}

Table 5. Ab initio single-crystal, directionally averaged and aggregate seismic properties of sapphirine-442 ($Mg_4Al_8Si_2O_{20}$) and sapphirine-351 ($Mg_3Al_{10}SiO_{20}$).

Sapphirine-442		Sapphirine-351	
$V_{S,MIN}$ (Km/s)	4.45	$V_{S,MIN}$ (Km/s)	4.63
$V_{S,MAX}$ (Km/s)	6.21	$V_{S,MAX}$ (Km/s)	6.46
u_1 (Km/s)	5.21	u_1 (Km/s)	5.32
u_2 (Km/s)	5.79	u_2 (Km/s)	5.98
u_3 (Km/s)	9.34	u_3 (Km/s)	9.62
$V_{S,VRH}$ (Km/s)	5.47	$V_{S,VRH}$ (Km/s)	5.61
$V_{P,VRH}$ (Km/s)	9.34	$V_{P,VRH}$ (Km/s)	9.62
K_V (GPa)	160.36	K_V (GPa)	173.27
K_R (GPa)	159.16	K_R (GPa)	172.78
K_{VRH} (GPa)	159.76	K_{VRH} (GPa)	173.02
μ_V (GPa)	104.70	μ_V (GPa)	112.01
μ_R (GPa)	97.06	μ_R (GPa)	103.20
μ_{VRH} (GPa)	100.88	μ_{VRH} (GPa)	107.60
E (GPa)	249.97	E (GPa)	267.32
ν_P	0.239	ν_P	0.243
ρ_0 (g/cm^3)	3.370	ρ_0 (g/cm^3)	3.419

Notes: $V_{S,MIN}$, $V_{S,MAX}$ = single-crystal slowest and fastest shear-wave velocities; u_1, u_2 = directionally averaged shear-wave velocities, u_3 = directionally averaged longitudinal-wave velocity; $V_{S,VRH}$, $V_{P,VRH}$ = Voigt-Reuss-Hill aggregate shear and longitudinal seismic velocities; K_V, K_R, K_{VRH} = Voigt, Reuss and Voigt-Reuss-Hill bulk moduli; μ_V, μ_R, $_{KVRH}$ = Voigt, Reuss and Voigt-Reuss-Hill shear moduli; E = Young's modulus; ν_P = Poisson's ratio; ρ_0 = density at the athermal limit (i.e. P = 0 GPa and T=0K).

Table 6. Thermochemical reference data for the atoms of interest in this study.

Species	$H^0_{f,Ai,0}$ (kJ/mol)	$\Delta H_{element,i,0\rightarrow 298.15}$ (kJ/mol)	E_{Ai} (hartree)
Si	445.668	3.2180	–289.293670
O	246.790	4.3415	–75.057906
Mg	145.900	4.9980	–200.014400
Al	327.300	4.5390	–242.283402

Notes: $H^0_{f,0}$ = enthalpy of formation of the gaseous atom from the stable element at T = 0 K, P = 1 bar (NIST-JANAF Tables; Chase 1998). $\Delta H_{element,i,0\rightarrow 298.15}$ is the enthalpy difference between T = 298. 15 K and T = 0 K for the monoatomic element (NIST-JANAF Tables; Chase 1998). E_{Ai} is the electronic energies of the gaseous atoms yielding a correct heat content of the constituent oxides at standard state in the compositional system $MgO\text{-}Al_2O_3\text{-}SiO_2$: the results obtained by Robie and Hemingway (1995) for periclase, Ditmars et al. (1982) for corundum and Richet et al. (1982) for quartz-α are taken as reference values (see Table 7).

Table 7. Thermochemical data for heat content calculation of sapphirine-442 ($Mg_4Al_8Si_2O_{20}$) and sapphirine-351 ($Mg_3Al_{10}SiO_{20}$).

Substance	D_0 (kJ/mol)	$E_{0,crystal}$ (hartree)	$E_{ZPE,crystal}$ (kJ/mol)	$H_{vib,298.15}$ (kJ/mol)	$H^0_{f,298.15}$ / B3LYP (kJ/mol)	$H°_{f,298.15}$ / Expt. (kJ/mol)	Ref.
MgO (periclase)	989.8	–275.454828	14.5	19.5	–601.4	–601.6	1, 2
α-Al_2O_3 (corundum)	3058.7	–710.922481	44.6	54.6	–1675.7	–1675.7 ± 1.2	1, 3, 4
α-SiO_2 (quartz)	1845.0	–440.123389	29.4	36.3	–910.7	–910.7	1, 5, 6
α-Mg_2SiO_4 (forsterite)	3883.4	–991.055720	59.1	75.7	–2172.7	–2173.0	1, 2
$Mg_4Al_8Si_2O_{20}$ (sapphirine-442)	20113.5	–4825.844937	298.7	374.6	–11158.0 (–11088.0)[a]	–11005 ± 33.5[b]	1, 7
$Mg_3Al_{10}SiO_{20}$ (sapphirine-351)	20351.7	–4821.194682	299.5	374.1	–11335.3 (–11203.3)[a]	–11106 ± 8.0[c]	1, 7

Notes: (1) this work; (2) Robie and Hemingway (1995); (3) Ditmars et al. (1982) ; (4) NIST-JANAF Tables (Chase 1998); (5) Ottonello et al., (2009b); (6) Richet et al. (1982); (7) Kiseleva (1976). [a] Optimized value according to MAS phase topology (see text for details). [b] Value measured on a synthetic disordered sample of formula $Mg_4Al_8Si_2O_{20}$. [c] Value measured on a natural ordered sample of formula $Mg_{3.5}Al_{9.0}Si_{1.5}O_{20}$.

Table 8. Ab initio B3LYP thermodynamic and thermophysical data for sapphirine-442 ($Mg_4Al_8Si_2O_{20}$) and sapphirine-351 ($Mg_3Al_{10}SiO_{20}$).

	Sapphirine-442	Sapphirine-351
V^0_{298} (cc/mol)	204.879	202.387
S^0_{298} (J/mol×K)	407.0	397.6
$\Delta_f H^0_{298}$ (kJ/mol)	–11088.0	–11203.3
K_0 (GPa)	158.73	172.33
K'_0	4.68	4.28
$(dK/dT)_P$ (bar/K)	–210.2	–188.0
$\alpha_0 \times 10^9$	9.0302	6.0817
$\alpha_1 \times 10^5$	1.0411	1.5709
$\alpha_2 \times 10^3$	14.0340	8.2836
α_3	–6.4469	–4.3554
α_4	814.288	547.232
a	791.61	789.73
$b \times 10^3$	65.455	60.300
$c \times 10^{-5}$	–181.750	–91.751
d	–481.63	–782.10
$e \times 10^{-8}$	–9.1576	–31.847
$f \times 10^6$	3.4196	13.270
$g \times 10^9$	–2.0517	–5.1473

Notes: V^0_{298} = molar volume at standard state (T=298.15 K and P = 1bar); S^0_{298} = standard state entropy; $\Delta_f H°_{298}$ = enthalphy of formation from the elements at standard state; K_0 = static bulk modulus; K'_0 = pressure derivative of bulk modulus; $(dK/dT)_P$ = isobaric temperature derivative of bulk modulus; α_0, α_1, α_2, α_3, α_4 = numerical coefficients of the polynomial function for thermal expansion (see Eq. 18); a, b, c, d, e, f, g = numerical coefficients of the polynomial function for isobaric heat capacity (C_P) (see Eq. 21).

Table 9. Standard state thermodynamic properties of sapphirine end-members at 1 bar, 298.15 K.

$Mg_4Al_8Si_2O_{20}$ (sapphirine-442)	$\Delta_fH^0_{298}$ (kJ/mol)	S^0_{298} (J/mol×K)	V^0_{298} (cc/mol)
this work	–11088.028	406.975	204.879
Kiseleva (1976)	–11005.6 ± 33.5	411.7056	-
Holland & Powell (1998)	–11014.08	440.00	198.70
Logvinkov et al. (2001)	–11107.497	390.34172	-
Kelsey et al. (2004)	–11003.38	450.00	199.05
Podlesskii et al. (2008)	–11018.469[a] (–11003.035)[b]	413.75[a] (425.32)[b]	198.61[a] (198.61)[b]
Holland & Powell (2011)	–11022.40	425.50	199.00
$Mg_3Al_{10}SiO_{20}$ (sapphirine-351)	$\Delta_fH^0_{298}$ (kJ/mol)	S^0_{298} (J/mol×K)	V^0_{298} (cc/mol)
this work	–11203.294	397.575	202.387
Kelsey et al. (2004)	–11138.46	420.00	197.51
Podlesskii et al. (2008)	–11168.243[a] (–11181.724)[b]	379.67[a] (367.94)[b]	196.67[a] (196.51)[b]
Holland & Powell (2011)	–11135.69	419.50	197.50

Notes: V^0_{298} = molar volume at standard state (T=298.15 K and P = 1bar); S^0_{298} = standard state entropy; $\Delta_fH°_{298}$ = enthalphy of formation from the elements at standard state; a = end-member properties for the ideal solid solution; b = end-member properties for the non-ideal solid solution.